Learning Structured Representations with Hyperbolic Embeddings

Aditya Sinha[*] [†]
University of Illinois, Urbana-Champaign
as146@illinois.edu

Siqi Zeng[*]
University of Illinois, Urbana-Champaign
siqi6@illinois.edu

Makoto Yamada
Okinawa Institute of Science and Technology
makoto.yamada@oist.jp

Han Zhao
University of Illinois, Urbana-Champaign
hanzhao@illinois.edu

Abstract

Most real-world datasets consist of a natural hierarchy between classes or an inherent label structure that is either already available or can be constructed cheaply. However, most existing representation learning methods ignore this hierarchy, treating labels as permutation invariant. Recent work [104] proposes using this structured information explicitly, but the use of Euclidean distance may distort the underlying semantic context [8]. In this work, motivated by the advantage of hyperbolic spaces in modeling hierarchical relationships, we propose a novel approach `HypStructure`: a Hyperbolic Structured regularization approach to accurately embed the label hierarchy into the learned representations. `HypStructure` is a simple-yet-effective regularizer that consists of a hyperbolic tree-based representation loss along with a centering loss. It can be combined with any standard task loss to learn *hierarchy-informed* features. Extensive experiments on several large-scale vision benchmarks demonstrate the efficacy of `HypStructure` in reducing distortion and boosting generalization performance, especially under low-dimensional scenarios. For a better understanding of structured representation, we perform an eigenvalue analysis that links the representation geometry to improved Out-of-Distribution (OOD) detection performance seen empirically. The code is available at `https://github.com/uiuctml/HypStructure`.

1 Introduction

Real-world datasets, such as ImageNet [72] and CIFAR [45], often exhibit a natural hierarchy or an inherent label structure that describes a structured relationship between different classes in the data. In the absence of an existing hierarchy, it is often possible to cheaply construct or infer this hierarchy from the label space directly [64]. However, the majority of existing representation learning methods [43, 7, 95, 29, 87, 33, 27, 39] treat the labels as permutation invariant, ignoring this semantically-rich hierarchical label information. Recently, Zeng et al. [104] offer a promising approach to embed the tree-hierarchy explicitly in representation learning using a tree-metric-based regularizer, leading to improvements in generalization performance. The approach uses a computation of shortest paths between two classes in the tree hierarchy to enforce the same structure in the feature space, by means of a **Co**phenetic **C**orrelation **C**oefficient (CPCC) [79] based regularizer. However, their approach uses the ℓ_2 distance in the Euclidean space, distorting the parent-child representations in the hierarchy [70, 50] owing to the bounded dimensionality of the Euclidean space [8].

[*]Authors contributed equally.
[†]Now at Netflix Inc.

Hyperbolic geometry has recently gained growing interest in the field of representation learning [66, 67]. Hyperbolic spaces can be viewed as the continuous analog of a tree, allowing for embedding tree-like data in finite dimensions with minimal distortion [44, 73, 75, 24]. Unlike Euclidean spaces with zero curvature and spherical spaces with positive curvature, the hyperbolic spaces have negative curvature enabling the length to grow exponentially with its radius. Owing to these advantages, hyperbolic geometry has been used for various applications such as natural language processing [52, 73, 16], image classification [40, 103, 18], object detection [46, 21], action retrieval [55], and hierarchical clustering [100]. However, the aim of using hyperbolic geometry in these approaches is often to *implicitly* leverage the hierarchical nature of the data.

In this work, given a label hierarchy, we argue that accurately and *explicitly* embedding the hierarchical information into the representation space has several benefits, and for this purpose, we propose `HypStructure`, a hyperbolic label-structure based regularization approach that extends the proposed methodology in [104] for semantically structured learning in the hyperbolic space. `HypStructure` can be easily combined with any standard task loss for optimization, and enables the learning of discriminative and *hierarchy-informed* features. In summary, our contributions are as follows:

- We propose `HypStructure` and demonstrate its effectiveness in the supervised hierarchical classification tasks on three real-world vision benchmark datasets, and show that our proposed approach is effective in both training from scratch, or fine-tuning if there are resource constraints.
- We qualitatively and quantitatively assess the nature of the learned representations and demonstrate that along with the performance gains, using `HypStructure` as a regularizer leads to more interpretable as well as tree-like representations as a side benefit. The low-dimensional representative capacity of hyperbolic geometry is well-known [6], and interestingly, we observe that training with `HypStructure` allows for learning extremely low-dimensional representations with distortion values lower than even their corresponding high-dimensional Euclidean counterparts.
- We argue that representations learned with an underlying hierarchical structure are beneficial not only for the in-distribution (ID) classification tasks but also for Out-of-distribution (OOD) detection tasks. We empirically demonstrate that learning ID representations with `HypStructure` leads to improved OOD detection on 9 real-world OOD datasets without sacrificing ID accuracy [106].
- Inspired by the improvements in OOD detection, we provide a formal analysis of the eigenspectrum of the in-distribution *hierarchy-informed* features learned with CPCC-style structured regularization methods, thus leading to a better understanding of the behavior of structured representations in general.

2 Preliminaries

In this section, we first provide a background of structured representation learning and then discuss the limited representation capacity of the Euclidean space for hierarchical information, which serves as the primary motivation for our work.

2.1 Background

Structured representation learning [104] breaks the permutation invariance of flat representation learning by incorporating a hierarchical regularization term with a standard classification loss. The regularization term is specifically designed to enforce class-conditioned grouping or partitioning in the feature space, based on a given hierarchy.

More specifically, given a weighted tree $\mathcal{T} = (V, E, e)$ with vertices V, edges E and edge weights e, let us compute a tree metric $d_{\mathcal{T}}$ for any pair of nodes $v, v' \in V$, as the weighted length of the shortest path in $\mathcal{T}$ between v and v'. For a real world dataset $\mathcal{D} = \{(\boldsymbol{x}_i, y_i)\}_{i=1}^{N}$, we can specify a *label tree* $\mathcal{T}$ where a node $v_i \in V$, v_i corresponds to a subset of classes, and $\mathcal{D}_i \subseteq \mathcal{D}$ denote the subset of data points with class label v_i. We denote dataset distance between $\mathcal{D}_i$ and $\mathcal{D}_j$ as $\rho(v_i, v_j) = d\left(\mathcal{D}_i, \mathcal{D}_j\right)$, where $d(\cdot, \cdot)$ is any distance metric in the feature space, varied by design.

With a collection of tree metric $d_\mathcal{T}$ and dataset distances ρ, we can use the Cophenetic Correlation Coefficient (CPCC) [79], inherently a Pearson's correlation coefficient, to evaluate the correspondence between the nodes of the tree, and the features in the representation space. Let $\overline{d_\mathcal{T}}, \overline{\rho}$ denote the mean of the collection of distances, then CPCC is defined as

$$\text{CPCC}(d_\mathcal{T}, \rho) := \frac{\sum_{i<j}(d_\mathcal{T}(v_i, v_j) - \overline{d_\mathcal{T}})(\rho(v_i, v_j) - \overline{\rho})}{(\sum_{i<j}(d_\mathcal{T}(v_i, v_j) - \overline{d_\mathcal{T}})^2)^{1/2}(\sum_{i<j}(\rho(v_i, v_j) - \overline{\rho})^2)^{1/2}}. \tag{1}$$

For the supervised classification task, we consider the training set $\mathcal{D}_{\text{tr}}^{\text{in}} = \{(\boldsymbol{x}_i, y_i)\}_{i=1}^N$ and we aim to learn the network parameter θ for a feature encoder $f_\theta : \mathcal{X} \to \mathcal{Z}$, where $\mathcal{Z} \subseteq \mathbb{R}^d$ denotes the representation/feature space. For structured representation learning, the feature encoder is usually followed by a classifier g_w, and the parameters θ, w are learnt by minimizing $\mathcal{L}$ along with a standard *flat* (non-hierarchical) classification loss, for instance, Cross-Entropy (`CE`) or Supervised Contrastive (`SupCon`) [39] loss, with the structured regularization term as:

$$\mathcal{L}(\mathcal{D}) = \sum_{(\boldsymbol{x},y)\in\mathcal{D}} \ell_{\text{Flat}}(\boldsymbol{x}, y, \theta, w) - \alpha \cdot \text{CPCC}(d_\mathcal{T}, \rho). \tag{2}$$

Using a composite objective as defined in Equation (2), we can enforce the distance relationship between a pair of representations in the feature space, to behave similarly to the tree metric between the same vertices. For instance, consider a simple label tree with a root node, a coarse level, and a fine level, where subsets of fine classes share the same coarse parent. For this hierarchy, we would expect the fine classes of the same parents (e.g., *apple* and *banana* are *fruits*) to have closer representations in the feature space, whereas fine classes with different coarse parents (e.g., an *apple* is a *fruit* and a *tulip* is a *flower*) should be further apart. The learned structure-informed representations reflect these hierarchical relationships and lead to interpretable features with better generalization [104].

2.2 ℓ_2-CPCC

Equation (1) offers the flexibility of designing a metric to measure the similarity between two data subsets, and [104] define the *Euclidean dataset distance* as $\rho_{\ell_2}(\mathcal{D}_i, \mathcal{D}_j) := \|\frac{1}{|\mathcal{D}_i|}\sum_{\boldsymbol{x}\in\mathcal{D}_i} f(\boldsymbol{x}) - \frac{1}{|\mathcal{D}_j|}\sum_{\boldsymbol{x}'\in\mathcal{D}_j} f(\boldsymbol{x}')\|_2$. The distance between datasets is thus the ℓ_2 distance between two Euclidean *centroids* of their class-conditioned representations, which is unsuitable for modeling *tree-like* data [8]. Additionally, this regularization approach in [104] is applied only to the leaf nodes of $\mathcal{T}$ for efficiency. However, this leaf-only formulation of the CPCC offers an *approximation* of the structured information, since the distance between non-leaf nodes is not restricted explicitly by the regularization. This approximation, therefore, leads to a loss of information contained in the original hierarchy $\mathcal{T}$. Actually, it is impossible to embed $d_\mathcal{T}$ into ℓ_2 exactly. Or more formally, there exists no bijection φ such that $d_\mathcal{T}(\varphi(\boldsymbol{z}_i), \varphi(\boldsymbol{z}_j)) = \|\boldsymbol{z}_i - \boldsymbol{z}_j\|_2$ irrespective of how large the feature dimension d is. We provide two such examples for a toy label tree in Figure 1, below.

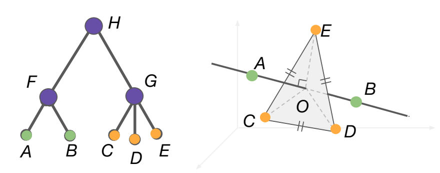

Figure 1: (left) An unweighted label tree with two coarse nodes: F, G. F contains two fine classes A, B and G contains three fine classes C, D, E. We cannot embed this in ℓ_2 exactly (right).

Example 1. We intend to embed all nodes in $\mathcal{T}$, including purple internal nodes. Notice that G, C, D, E is a star graph centered at G. Since $CG = DG = 1, CD = 2$, by triangle inequality C, D, G must be on the same line where G is the center of CD. Similarly, G must be at the center of DE. Hence, the location of E must be at C, which contradicts the uniqueness of all nodes in $\mathcal{T}$.

Example 2. As an easier problem, let us only embed leaf nodes into the Euclidean space as shown in Figure 1. Since $CD = DE = CE = 2$, they must be on a plane with an equilateral triangle $\triangle_{CDE}$ in Euclidean geometry. Then all the green classes have the same distance 4 to each yellow class. Therefore, A, B must be on the line perpendicular to $\triangle_{CDE}$ and intersecting the plane with O, which is the barycenter of $\triangle_{CDE}$. Due to the uniqueness and symmetry of A, B, we must have $AO = BO = 1$ to satisfy $AB = 2$. $AO = 1, OE = \frac{2\sqrt{3}}{3}, AE = 4$ which contradicts the Pythagorean Theorem.

Since we cannot embed an arbitrary tree $\mathcal{T}$ into ℓ_2 without distortion, it would also affect the optimization of the ℓ_2-CPCC in a classification problem, where the tree weights encode knowledge

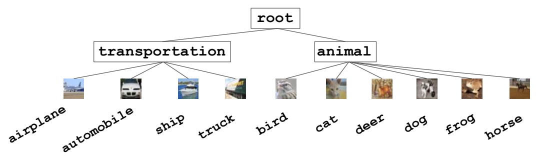

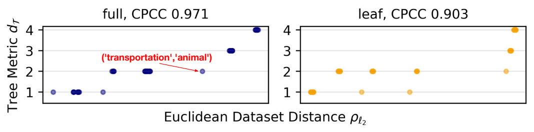

Figure 2: Using ℓ_2-CPCC for structured representation on CIFAR10. CIFAR10 hierarchy (left) has a three level structure with 13 vertices. For a 512-dimensional embedding, we apply ℓ_2-CPCC either for the full tree (middle) or the leaf nodes only (right) and plot the ground truth tree metric against pairwise Euclidean centroid distances of the learnt representation. The optimal train CPCC is 1.

of class similarity. To verify our claims, we consider the optimization of 512-dimensional ℓ_2-CPCC structured representations for CIFAR10 [45]. The CIFAR10 dataset consists of a small label hierarchy as shown in Figure 2 (left). The optimal CPCC is achieved when each tree metric value corresponds to a single ρ_{ℓ_2}. However, in Figure 2 (right), even with an optimization of the ℓ_2-CPCC loss for the entire tree, we observe a sub-optimal train CPCC less than 1, where the distance between two coarse nodes, *transportation* and *animal*, is far away from the desired solution. Furthermore, optimization of the CPCC loss for only the leaf nodes, leads to an even larger distortion of the tree metrics.

3 Methodology

Hyperbolic spaces are more suitable for embedding hierarchical relationships with low distortion [75] and low dimensions. Hence, motivated by the aforementioned challenges, we propose a **Hyp**erbolic **Structure**d regularizer for *hierarchy-informed* representation learning. We begin with the basics of hyperbolic geometry, followed by the detailed methodology of our proposed approach.

3.1 Hyperbolic Geometry

Hyperbolic spaces are non-Euclidean spaces with negative curvature where given a fixed point and a line, there exist infinitely many parallel lines that can pass through this point. There are several commonly used isometric hyperbolic models [4]. For this work, we mainly use the Poincaré Ball model.

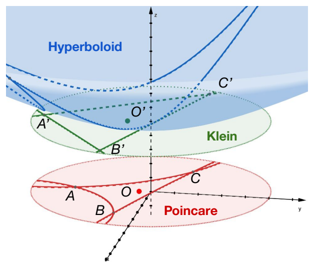

Figure 3: Lines on different models for 2-dimensional hyperbolic space.

Definition 3.1 (Manifold)**.** A *manifold* $\mathcal{M}$ is a set of points $\boldsymbol{z}$ that are locally Euclidean. Every point $\boldsymbol{z}$ of the manifold $\mathcal{M}$ is attached to a *tangent space* $\mathcal{T}_{\boldsymbol{z}}\mathcal{M}$, which is a vector space over the reals of the same dimensionality as $\mathcal{M}$ that contain all the possible directions that can tangentially pass through $\boldsymbol{z}$.

Definition 3.2 (Poincaré Ball Model)**.** Given c as a constant, the Poincaré ball model $(\mathbb{B}_c^d, \mathfrak{g}_B)$ is defined by a manifold of an open ball $\mathbb{B}_c^d = \{\boldsymbol{z} \in \mathbb{R}^d : c\|\boldsymbol{z}\|^2 < 1\}$ and metric tensor $\mathfrak{g}_B$ that defines an inner product of $\mathcal{T}_{\boldsymbol{z}}\mathbb{B}_c^d$. The model is equipped with the distance [88] as

$$d_{\mathbb{B}_c}(\boldsymbol{z}_1, \boldsymbol{z}_2) = \frac{2}{\sqrt{c}} \tanh^{-1}\left(\sqrt{c}\left\|\frac{-(1+2c\langle -\boldsymbol{z}_1, \boldsymbol{z}_2\rangle + c\|\boldsymbol{z}_2\|^2)\boldsymbol{z}_1 + (1-c\|\boldsymbol{z}_1\|^2)\boldsymbol{z}_2}{1-2c\langle \boldsymbol{z}_1, \boldsymbol{z}_2\rangle + c^2\|\boldsymbol{z}_1\|^2\|\boldsymbol{z}_2\|^2}\right\|\right). \quad (3)$$

For $c \to 0$, we can recover the properties of the Euclidean geometry since $\lim_{c\to 0} d_{\mathbb{B}_c}(\boldsymbol{z}_1, \boldsymbol{z}_2) = 2\|\boldsymbol{z}_1 - \boldsymbol{z}_2\|$. Since $\mathcal{T}_{\boldsymbol{z}}\mathbb{B}_c^d$ is isomorphic to $\mathbb{R}^d$, we can connect vectors in Euclidean space and hyperbolic space with the bijection between $\mathcal{T}_{\boldsymbol{z}}\mathbb{B}_c^d$ and $\mathbb{B}_c^d$ [88]. For $\boldsymbol{z} = \boldsymbol{0}$, the *exponential map* $\exp_{\boldsymbol{0}}^c : \mathcal{T}_{\boldsymbol{z}}\mathbb{B}_c^d \to \mathbb{B}_c^d$ and *logarithm map* $\log_{\boldsymbol{0}}^c : \mathbb{B}_c^d \to \mathcal{T}_{\boldsymbol{z}}\mathbb{B}_c^d$ have the closed form of

$$\exp_{\boldsymbol{0}}^c(\boldsymbol{v}) = \tanh\left(\sqrt{c}\|\boldsymbol{v}\|\right)\frac{\boldsymbol{v}}{\sqrt{c}\|\boldsymbol{v}\|}, \quad \log_{\boldsymbol{0}}^c(\boldsymbol{u}) = \frac{1}{\sqrt{c}}\tanh^{-1}\left(\sqrt{c}\|\boldsymbol{u}\|\right)\frac{\boldsymbol{u}}{\|\boldsymbol{u}\|}. \quad (4)$$

Alternatively, to guarantee the correctness of Poincaré distance computation, we can also process any Euclidean vector with a clipping module [66]

$$\operatorname{clip}^c(\boldsymbol{v}) = \begin{cases} \boldsymbol{v}, & \text{if } \|\boldsymbol{v}\| < 1/\sqrt{c} \\ \left(\frac{1}{\sqrt{c}} - \epsilon\right)\frac{\boldsymbol{v}}{\|\boldsymbol{v}\|}, & \text{otherwise} \end{cases}, \quad (5)$$

so the clipped vector is within the Poincare disk. We set ϵ as a small positive number in practice.

Definition 3.3 (Klein Model)**.** Klein model $(\mathbb{K}_c^d, \mathfrak{g}_K)$ consists of an $1/\sqrt{c}$-radius open ball $\mathbb{K}_c^d = \{\boldsymbol{z} \in \mathbb{R}^d : c\|\boldsymbol{z}\|^2 < 1\}$ and a metric tensor $\mathfrak{g}_K$ different from $\mathfrak{g}_B$. Similar to the mean computation in Euclidean space, let $\gamma_i = 1/\sqrt{1 - c\|\boldsymbol{z}_i\|^2}$, the Einstein midpoint of a group of Klein vectors $\boldsymbol{z}_1, \ldots \boldsymbol{z}_n \in \mathbb{K}_c^d$ has a simple expression of a weighted average

$$\text{HypAve}_K(\boldsymbol{z}_1, \ldots \boldsymbol{z}_n) = \sum_{i=1}^{n} \gamma_i \boldsymbol{z}_i \Big/ \sum_{i=1}^{n} \gamma_i. \tag{6}$$

We illustrate the relationship between the different hyperbolic models in Figure 3. The hyperboloid space models d-dimensional hyperbolic geometry on a $d+1$-dimensional space. When $d = 2$, the Klein model is the tangent plane of the hyperboloid model at $(0, 0, 1)$, and the Poincaré disk shares the same support as the Klein disk, although shifted downwards and centered at the origin. Given a triangle on the hyperboloid model, its projection on the Klein model preserves the straight sides, but the projection of a line on the Poincaré model is a part of a circular arc or the diameter of the disk. Let $\boldsymbol{z}_{\mathbb{B}}, \boldsymbol{z}_{\mathbb{K}}$ be coordinates of $\boldsymbol{z}$ under Poincaré and Klein model respectively, the prototype operations on $\mathbb{B}_c^d$ require transformations between $\mathbb{B}_c^d$ and $\mathbb{K}_c^d$ as

$$\boldsymbol{z}_{\mathbb{B}} = \frac{\boldsymbol{z}_{\mathbb{K}}}{1 + \sqrt{1 - c\|\boldsymbol{z}_{\mathbb{K}}\|^2}}, \quad \boldsymbol{z}_{\mathbb{K}} = \frac{2\boldsymbol{z}_{\mathbb{B}}}{1 + c\|\boldsymbol{z}_{\mathbb{B}}\|^2}. \tag{7}$$

For example, in Figure 3, O' is the HypAve_{K} of A', B', C', and can be mapped back to the Poincaré disk to get the Poincaré prototype (HypAve_{B}) O of points A, B, C by a change of coordinates.

3.2 `HypStructure`: Hyperbolic Structured Regularization

At a high level, `HypStructure` uses a combination of two losses: a Hyperbolic Cophenetic Correlation Coefficient Loss (`HypCPCC`)), and a Hyperbolic centering loss (`HypCenter`) for embedding the hierarchy in the representation space. Below we describe the two components of `HypStructure`. The pseudocode of `HypStructure` is shown in Algorithm 1 in Appendix B.2.

HypCPCC (Hyperbolic Cophenetic Correlation Coefficient): We extend the ℓ_2-CPCC methodology in [104] to the hyperbolic space in `HypCPCC`. Three major steps of `HypCPCC` are (i) map Euclidean vectors to Poincaré space (ii) compute class prototypes (iii) use Poincaré distance for CPCC. Specifically, we first project each $\boldsymbol{z}_i \in \mathbb{R}^d$ to $\mathbb{B}_c^d$, and compute the Poincaré centroid for each vertex of $\mathcal{T}$ using hyperbolic averaging as shown in Equation (6) and Equation (7). Alternatively, we can also compute Euclidean centroids $\overline{\boldsymbol{z}} = \frac{1}{|\mathcal{D}_i|}\sum_{\boldsymbol{z} \in \mathcal{D}_i} \boldsymbol{z}$ for each vertex, and project each $\overline{\boldsymbol{z}} \in \mathbb{R}^d$ to $\mathbb{B}_c^d$ either by $\exp_{\mathbf{0}}^c$ or clip^c. After the computation of hyperbolic centroids, we use the pairwise distances between all vertex pairs in $\mathcal{T}$ in the Poincaré ball, to compute the `HypCPCC` loss using Equation (1) by setting $\rho = d_{\mathbb{B}_c}$.

HypCenter (Hyperbolic Centering): Inspired by Sarkar's low-distortion construction [75] that places the root node of a tree at the origin, we propose a centering loss for this positioning, that enforces the representation of the root node to be close to the center of the Poincaré disk, and the representations of its children to be closer to the border of Poincaré disk. We enforce this constraint by minimizing the norm of the hyperbolic representation of the root node as $\ell_{\text{center}} = \|\text{HypAve}_B(\exp_{\mathbf{0}}^c(\boldsymbol{z}_1), \ldots, \exp_{\mathbf{0}}^c(\boldsymbol{z}_N))\|$. Alternatively, for centroids computed in the Euclidean space and mapped to the Poincaré disk, we minimize $\ell_{\text{center}} = \left\|1/N\sum_{i=1}^{N} f_\theta(\boldsymbol{x}_i)\right\|$ directly due to the monotonicity of $\tanh(\cdot)$ in the exponential map.

Finally, for $\alpha, \beta > 0$, we can learn the *hierarchy-informed* representations by minimizing

$$\mathcal{L}(\mathcal{D}) = \sum_{(\boldsymbol{x},y)\in\mathcal{D}} \ell_{\text{Flat}}(\boldsymbol{x}, y, \theta) - \alpha \cdot \text{HypCPCC}(d_{\mathcal{T}}, d_{\mathbb{B}_c}) + \beta \cdot \ell_{\text{center}}(\boldsymbol{x}, \theta), \tag{8}$$

where ℓ_{Flat} is a standard classification loss, such as the `CE` loss or the `SupCon` loss.

Time Complexity: In a batch computation setting with a batch size b and the number of classes (leaf nodes) as k, the computational complexity for a `HypStructure` computation to embed the full tree will still be $O(d \cdot \min\{b^2, k^2\})$, which is the same as the complexity of a Euclidean *leaf-only* CPCC. The additional knowledge gained from internal nodes allows us to reason about the relationship between higher-level concepts, and the hyperbolic representations help in achieving a low distortion of hierarchical information for better performance in downstream tasks.

4 Experiments

We conduct extensive experiments on several large-scale image benchmark datasets to evaluate the performance of `HypStructure` as compared to the Flat and ℓ_2-CPCC baselines for hierarchy embedding, classification, and OOD detection tasks.

Datasets and Setup Following the common benchmarks in the literature, we consider three real-world vision datasets, namely CIFAR10, CIFAR100 [45] and ImageNet100 [59] for training, which vary in scale, number of classes, and number of images per class. We construct the ImageNet100 dataset by sampling 100 classes from the ImageNet-1k [72] dataset following [59]. For CIFAR100, a three-level hierarchy is available with the dataset release [45]. Since no hierarchy is available for the CIFAR10 and ImageNet100 datasets, we construct a hierarchy for CIFAR10 manually in Figure 2. For ImageNet100, we create a subtree from the WordNet [19] given 100 classes as leaves. More details regarding the datasets, network, training and setup are provided in the Appendix B.4.

4.1 Quality of Hierarchical Information

Table 1: Evaluation of hierarchical information distortion and classification accuracy using `SupCon` [39] as ℓ_{Flat}. All metrics are reported as mean (standard deviation) over 3 seeds.

Dataset (Backbone)	Method	Distortion of Hierarchy		Classification Accuracy	
		δ_{rel} (↓)	CPCC (↑)	Fine (↑)	Coarse (↑)
CIFAR10 (ResNet-18)	Flat	0.232 (0.001)	0.573 (0.002)	94.64 (0.12)	99.16 (0.04)
	ℓ_2-CPCC	0.174 (0.002)	0.966 (0.001)	94.47 (0.13)	98.91 (0.02)
	`HypStructure`	**0.094 (0.003)**	**0.992 (0.001)**	**94.79 (0.14)**	**99.18 (0.04)**
CIFAR100 (ResNet-34)	Flat	0.209 (0.002)	0.534 (0.119)	74.96 (0.14)	84.15 (0.19)
	ℓ_2-CPCC	0.213 (0.006)	**0.779 (0.002)**	76.07 (0.19)	85.28 (0.32)
	`HypStructure`	**0.127 (0.016)**	0.766 (0.007)	**76.68 (0.22)**	**86.01 (0.13)**
ImageNet100 (ResNet-34)	Flat	0.168 (0.003)	0.429 (0.002)	90.01 (0.07)	90.77 (0.11)
	ℓ_2-CPCC	0.213 (0.009)	0.834 (0.002)	89.57 (0.38)	90.34 (0.28)
	`HypStructure`	**0.134 (0.001)**	**0.841 (0.001)**	**90.12 (0.01)**	**90.84 (0.02)**

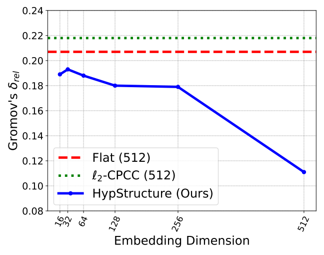

Figure 4: Evaluation of distortion vs feature dimensions for `HypStructure`.

First, to assess the *tree-likeness* of the learnt representations, we measure the Gromov's hyperbolicity δ_{rel} [23, 1, 38, 40] of the features in Table 1. Lower δ_{rel} indicates higher tree-likeness and a perfect tree metric space has $\delta_{rel} = 0$ (more details in Appendix B.5). To also evaluate the correspondence of the feature distances with ground truth tree metrics, we compute CPCC on test sets. We observe that `HypStructure` reduces distortion of hierarchical information over Flat by upto **59.4%** and over ℓ_2-CPCC by upto **45.4%**, while also consistently improving the test CPCC for most datasets.

We also perform a qualitative analysis of the learnt representations from `HypStructure` on the CIFAR10 dataset, and visualize them in a Poincaré disk using UMAP [57] in Figure 5a. We can observe clearly that the samples for fine classes arrange themselves in the Poincaré disk based on the hierarchy tree as seen in Figure 2, being closer to the classes which share a *coarse* class parent.

To examine the impact of feature dimension on the representative capacity of the hyperbolic space, we vary the feature dimension for `HypStructure` and compute the δ_{rel} for each learnt feature. Comparing the distortion of features with the Flat and ℓ_2-CPCC settings in Figure 4, we observe that δ_{rel} decreases consistently with increasing dimensions, implying that high dimension features using `HypStructure` are more tree-like, and better than Flat and ℓ_2-CPCCs' 512-dimension baselines.

4.2 Classification

Following [104], we treat leaf nodes in the hierarchy as *fine* classes and their parent nodes as *coarse* classes. To evaluate the quality of the learnt representations, we perform a classification task on the fine and coarse classes using a kNN-classifier following [27, 95, 5, 110] and report the performance on the three datasets in Table 1. We observe that `HypStructure` leads to upto **2.2%** improvements over Flat and upto **0.8%** improvements over ℓ_2-CPCC on both fine and coarse accuracy. We also visualize the learnt test features from Flat vs `HypStructure` on the CIFAR100 dataset using Euclidean t-SNE [89] and show the visualizations in Figure 5b and Figure 5c respectively. We observe that `HypStructure` leads to sharper and more discriminative representations in Euclidean space. Additionally, we see that the fine classes belonging to a coarse class (the same shades of colors)

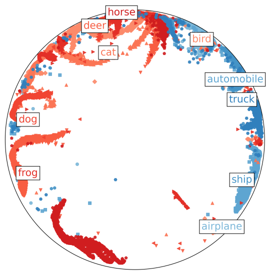

(a) Hyperbolic UMAP: `HypStructure`

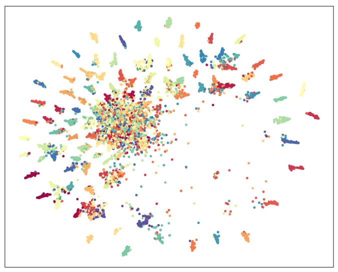

(b) Euclidean t-SNE: Flat

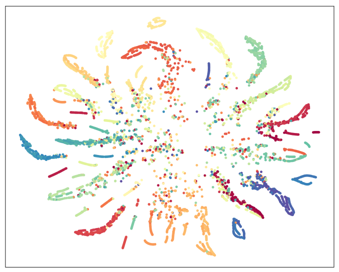

(c) Euclidean t-SNE: `HypStructure`

Figure 6: Left: Hyperbolic UMAP visualization of CIFAR10's `HypStructure` representation on Poincaré disk. Middle and Right: t-SNE visualization of learnt representations on CIFAR100.

which are semantically closer in the label hierarchy, are grouped closer and more compactly in the feature space as well, as compared to Flat. We also perform evaluations using the linear evaluation protocol [39] and observe an identical trend in the accuracy, we report these results in Appendix C.1.

4.3 OOD Detection

In addition to leveraging the hierarchy explicitly for the purpose of learning tree-like ID representations, we argue that a structured separation of features in the hyperbolic space as enforced by `HypStructure` is helpful for the OOD detection task as well. To verify our claim, we perform an exhaustive evaluation on 9 real-world OOD datasets and demonstrate that `HypStructure` leads to improvements in the OOD detection AUROC. We share more details below.

Method	**OOD Dataset AUROC (↑)**					**Overall AUROC**	
	SVHN	Textures	Places365	LSUN	iSUN	**Avg.(↑)**	**B.C.(↑)**
ProxyAnchor [41]	82.43	84.99	79.84	91.68	84.96	84.78	51.42
CE + SimCLR [94]	94.45	82.01	71.48	89.00	83.82	84.15	31.42
CSI [85]	92.65	86.47	76.27	83.78	**84.98**	84.83	40.00
CIDER [61]	95.16	90.42	73.43	96.33	82.98	87.67	60.00
SSD+ (SupCon) [76]	94.19	86.18	**79.90**	85.18	84.08	85.90	54.28
KNN+ (SupCon) [83]	92.78	88.35	77.58	89.30	82.69	86.14	40.00
ℓ_2-CPCC [104]	93.08	**90.45**	77.21	82.77	82.79	85.26	40.00
`HypStructure`	**95.97**	88.43	78.12	**97.01**	84.51	**88.81**	**82.85**

(a) OOD detection performance with CIFAR100 as ID dataset.

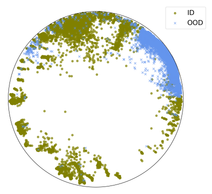

(b) CIFAR100 (ID) vs. SVHN (OOD).

Figure 7: Left: OOD detection score across various datasets on the CIFAR100 ID dataset. Right: Hyperbolic UMAP of the CIFAR100 (ID) test vs SVHN (OOD) test features learnt from `HypStructure` with a clear separation in the Poincaré disk.

4.3.1 Problem Setting

Out-of-distribution (OOD) data refers to samples that do not belong to the in-distribution (ID) and whose label set is disjoint from $\mathcal{Y}^{\text{in}}$ and therefore should not be predicted by the model. Therefore the goal of the OOD detection task is to design a methodology that can solve a binary problem of whether an incoming sample $\boldsymbol{x} \in \mathcal{X}$ is from $P_{\mathcal{X}}$ i.e. $y \in \mathcal{Y}^{\text{in}}$ (ID) or $y \notin \mathcal{Y}^{\text{in}}$ (OOD).

OOD datasets We evaluate on 5 OOD image datasets when CIFAR10 and CIFAR100 are used as the ID datasets, namely `SVHN` [65], `Places365` [109], `Textures` [9], `LSUN` [102], and `iSUN` [99], and 4 large scale OOD test datasets, specifically `SUN` [102], `Places365` [109], `Textures` [9] and `iNaturalist` [90] when ImageNet100 is used as the ID dataset. This subset of datasets is prepared by [59] and is created with overlapping classes from ImageNet-1k removed from these datasets to ensure there is no overlap in the distributions.

OOD detection scores While several scores have been proposed for the task of OOD detection, we evaluate our proposed method using the Mahalanobis score [76], computed by estimating the mean

Table 2: OOD detection AUROC with CIFAR10 and ImageNet100 as ID.

Method	**AUROC**	**Method**	**AUROC**
CIFAR10		**ImageNet100**	
SSD+	97.38	SSD+	92.46
KNN+	97.22	KNN+	92.74
ℓ_2-CPCC	76.67	ℓ_2-CPCC	91.33
`HypStructure`	**97.75**	`HypStructure`	**93.83**

and covariance of the in-distribution training features. The Mahalanobis score is defined as

$$s(\boldsymbol{x}) = (f(\boldsymbol{x}) - \mu)^\top \Sigma^{-1} (f(\boldsymbol{x}) - \mu), \tag{9}$$

where μ, Σ are the mean and covariance of in-distribution training features. [76] present the Mahalanobis score (eq. (9)) in a generalized version for multiple feature clusters. However, since they empirically observe that the single-cluster version achieves the highest performance [76], we will focus on this version. After computing the OOD detection scores, we measure the area under the receiver operating characteristic curve (AUROC) as the primary evaluation metric following [47, 76].

4.3.2 Main Results and Discussion

We report the AUROC averaged over all the OOD datasets (5 datasets for CIFAR10 and CIFAR100, 4 datasets for ImageNet100) in Figure 7a and Table 2 In addition to the Flat (`SupCon`) and ℓ_2-CPCC baselines, we also compare our method with other state-of-the-art methods (see Appendix C.3.1 for more details about existing OOD detection methods). We observe that `HypStructure` leads to a consistent improvement in the OOD detection score, with upto **2%** in average AUROC. We also report the dataset-wise OOD detection results for the CIFAR100 ID dataset in Table 7a along with Average AUROC. To remove the bias in the Average AUROC metric towards any single dataset, we also evaluate the Borda Count (B.C.) [58] and report the same, along with a detailed comparison with more OOD detection methods in Table 7a, and Tables 6 and 7 in the Appendix C.3. We observe that `HypStructure` ranks in the highest performing methods consistently, thereby demonstrating a higher Borda Count as well. We additionally visualize the CIFAR100 (ID) vs SVHN (OOD) features learnt from `HypStructure`, using a hyperbolic UMAP visualization in Figure 7b. We observe that training with `HypStructure` leads to an improvement in the separation of ID vs OOD features in the Poincaré disk.

Additional Experiments, Ablations and Visualizations: More experiments using hyperbolic contrastive losses and hyperbolic networks, ablation studies on each component of `HypStructure` and additional visualizations can be found in Appendix C.

5 Eigenspectrum Analysis of Structured Representations

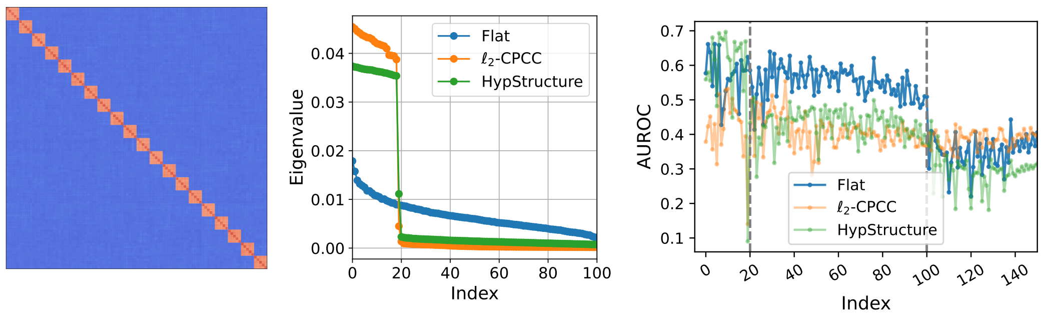

Figure 8: CIFAR100 as in-distribution dataset. Left (a): Hierarchical block pattern of K. Middle (b): Top 100 eigenvalues of K for different representation. Right (c): OOD detection for CIFAR100 vs. SVHN with the top k-th principal component.

As seen in Figure 7a, we observe a significant improvement in the OOD detection performance using `HypStructure` with the Mahalanobis score eq. (9). After training a composite loss with CPCC till convergence, let us denote the matrix of the normalized in-distribution trained feature as $Z \in \mathbb{R}^{n \times d}$. Naturally, we inspect the eigenvalue properties of Σ (i.e, Z), and observe that $K = Z^\top Z \in \mathbb{R}^{n \times n}$ exhibits a hierarchical block structure (Figure 8a) where the diagonal blocks have a significantly higher correlation than other off-diagonal values, leading us to the following theorem.

Theorem 5.1 (**Eigenspectrum of Structured Representation with Balanced Label Tree).** *Let $\mathcal{T}$ be a balanced tree with height H, such that each level has C_h nodes, $h \in [0, H]$. Let us denote each entry of K as r^h where h is the height of the lowest common ancestor of the row and the column sample. If $r^h \geq 0, \forall h$, then: (i) For $h = 0$, we have $C_0 - C_1$ eigenvalues $\lambda_0 = 1 - r^1$. (ii) For $0 < h \leq H - 1$, we have $C_h - C_{h+1}$ eigenvalues $\lambda_h = \lambda_{h-1} + (r^h - r^{h+1})\frac{C_0}{C_h}$. (iii) The last eigenvalue is $\lambda_H = \lambda_{H-1} + C_0 r^H$.*

We defer the eigenspectrum analysis for an arbitrary label tree to Appendix A. Theorem 5.1 implies a **phase transition pattern** in the eigenspectrum. There always exists a significant gap in the eigenvalues representing each level of nodes in the hierarchy, and the eigenvalues corresponding to the coarsest level are the highest in magnitude. CIFAR100 has a balanced three-level label hierarchy where each coarse label has five fine labels as its children. In Figure 8b, we visualize the eigenspectrum of CIFAR100 for `HypStructure`, ℓ_2-CPCC and the Flat objective. We observe a significant drop in the eigenvalues for features learnt from two hierarchical regularization approaches, ℓ_2-CPCC and `HypStructure`, at approximately the 20th largest eigenvector (which corresponds to the number of coarse classes), whereas these phase transitions do not appear for standard flat features. We also observe that the magnitude of coarse eigenvalues are approximately at the same scale.

In summary, Theorem 5.1 helps us to formally characterize the difference between flat and structured representations. CPCC style (eq. (1)) regularization methods can also be treated as dimensionality reduction techniques, where the structured features can be explained mostly by the coarser level features. For the OOD detection setting, this property differentiates the ID and OOD samples at the coarse level itself using a lower number of dimensions, and makes the OOD detection task easier. We visualize the OOD detection AUROC on SVHN (OOD) corresponding to the CIFAR100 (ID) features with the top$-k$ principal component for different methods, in Figure 8c. We observe that for features learnt using `HypStructure`, accurately embedding the hierarchical information leads to the top 20 eigenvectors (corresponding to the coarse classes) being the most informative for OOD detection. Recall that CIDER [61] is a state-of-the-art method proposed specifically for improving OOD detection by increasing inter-class dispersion and intra-class compactness. We note that CPCC style (eq. (1)) methods can be seen as a generalization of CIDER on higher-level concepts, where the same rules are applied for coarse labels as well, along with the fine classes. When the ID and OOD distributions are far enough, using coarse level feature might be sufficient for OOD detection.

6 Related Work

Learning with Label Hierarchy. Several recent works have explored how to leverage hierarchical information between classes for various purposes such as relational consistency [14], designing specific hierarchical classification architectures [101, 25, 68], hierarchical conditioning of the logits [13], learning order preserving embeddings [15], and improving classification accuracy [91, 86, 48, 49, 108, 34]. The proposed structural regularization framework in [104] offers an interesting approach to embed a tree metric to learn structured representations through an *explicit* objective term, although they rely on the ℓ_2 distance, which is less than ideal for learning hierarchies.

Hyperbolic Geometry. [66] first proposed using the hyperbolic space to learn hierarchical representations of symbolic data such as text and graphs by embedding them into a Poincaré ball. Since then, the use of hyperbolic geometry has been explored in several different applications. [40] proposed a hyperbolic image embedding for few-shot learning and person re-identification. [20] proposed hyperbolic neural network layers, enabling the development of hybrid architectures such as hyperbolic convolutional neural networks [78], graph convolutional networks [12], hyperbolic variational autoencoders [56] and hyperbolic attention networks [24]. Additionally, these hybrid architectures have also been explored for different tasks such as deep metric learning [18, 100], object detection [46] and natural language processing [16]. There have also been several investigations into the properties of hyperbolic spaces and models such as low distortion [75], small generalization error [84] and representation capacity [62]. However, none of these works have leveraged hyperbolic geometry for *explicitly* embedding a hierarchy in the representation space via structured regularization, and usually attempt to leverage the underlying hierarchy *implicitly* using hyperbolic models.

7 Discussion and Future Work

In this work, we introduce `HypStructure`, a simple-yet-effective structural regularization framework for incorporating the label hierarchy into the representation space using hyperbolic geometry. In particular, we demonstrate that accurately embedding the hierarchical relationships leads to empirical improvements in both classification as well as the OOD detection tasks, while also learning *hierarchy-informed* features that are more interpretable and exhibit less distortion with respect to the label hierarchy. We are also the first to formally characterize properties of *hierarchy-informed* features via an eigenvalue analysis, and also relate it to the OOD detection task, to the best of our knowledge. We acknowledge that our proposed method depends on the availability or construction of an external hierarchy for computing the HypCPCC objective. If the hierarchy is unavailable or contains noise, this could present challenges. Therefore, it is important to evaluate how injecting noisy hierarchies into CPCC-based methods impacts downstream tasks. While the current work uses the Poincaré ball model, exploring the representation trade-offs and empirical performances using other models of hyperbolic geometry in `HypStructure`, such as the Lorentz model [67] is an interesting future direction. Further theoretical investigation into establishing the error bounds of CPCC style structured regularization objectives is of interest as well.

Acknowledgement

SZ and HZ are partially supported by an NSF IIS grant No. 2416897. HZ would like to thank the support from a Google Research Scholar Award. MY was supported by MEXT KAKENHI Grant Number 24K03004. We would also like to thank the reviewers for their constructive feedback during the review process. The views and conclusions expressed in this paper are solely those of the authors and do not necessarily reflect the official policies or positions of the supporting companies and government agencies.

References

[1] Aaron B Adcock, Blair D Sullivan, and Michael W Mahoney. Tree-like structure in large social and information networks. In *2013 IEEE 13th international conference on data mining*, pages 1–10. IEEE, 2013.

[2] Abhijit Bendale and Terrance E Boult. Towards open set deep networks. In *CVPR*, 2016.

[3] Jorge Cadima, Francisco Lage Calheiros, and Isabel P. Preto. The eigenstructure of block-structured correlation matrices and its implications for principal component analysis. *Journal of Applied Statistics*, 37(4):577–589, April 2010.

[4] James W Cannon, William J Floyd, Richard Kenyon, Walter R Parry, et al. Hyperbolic geometry. *Flavors of geometry*, 31(59-115):2, 1997.

[5] Mathilde Caron, Ishan Misra, Julien Mairal, Priya Goyal, Piotr Bojanowski, and Armand Joulin. Unsupervised learning of visual features by contrasting cluster assignments. *Advances in neural information processing systems*, 33:9912–9924, 2020.

[6] Ines Chami, Adva Wolf, Da-Cheng Juan, Frederic Sala, Sujith Ravi, and Christopher Ré. Low-dimensional hyperbolic knowledge graph embeddings. *arXiv preprint arXiv:2005.00545*, 2020.

[7] Ting Chen, Simon Kornblith, Mohammad Norouzi, and Geoffrey Hinton. A simple framework for contrastive learning of visual representations. In *International conference on machine learning*, pages 1597–1607. PMLR, 2020.

[8] Wei Chen, Wenjie Fang, Guangda Hu, and Michael W Mahoney. On the hyperbolicity of small-world and treelike random graphs. *Internet Mathematics*, 9(4):434–491, 2013.

[9] Mircea Cimpoi, Subhransu Maji, Iasonas Kokkinos, Sammy Mohamed, and Andrea Vedaldi. Describing textures in the wild. In *Proceedings of the IEEE Conference on Computer Vision and Pattern Recognition*, pages 3606–3613, 2014.

[10] ED Cubuk, B Zoph, J Shlens, and QV Le. Randaugment: Practical data augmentation with no separate search. arxiv 2019. *arXiv preprint arXiv:1909.13719*.

[11] Ekin D Cubuk, Barret Zoph, Dandelion Mane, Vijay Vasudevan, and Quoc V Le. Autoaugment: Learning augmentation strategies from data. In *Proceedings of the IEEE/CVF conference on computer vision and pattern recognition*, pages 113–123, 2019.

[12] Jindou Dai, Yuwei Wu, Zhi Gao, and Yunde Jia. A hyperbolic-to-hyperbolic graph convolutional network. In *Proceedings of the IEEE/CVF conference on computer vision and pattern recognition*, pages 154–163, 2021.

[13] Jim Davis, Tong Liang, James Enouen, and Roman Ilin. Hierarchical classification with confidence using generalized logits. In *2020 25th International Conference on Pattern Recognition (ICPR)*, pages 1874–1881. IEEE, 2021.

[14] Jia Deng, Nan Ding, Yangqing Jia, Andrea Frome, Kevin Murphy, Samy Bengio, Yuan Li, Hartmut Neven, and Hartwig Adam. Large-scale object classification using label relation graphs. In David Fleet, Tomas Pajdla, Bernt Schiele, and Tinne Tuytelaars, editors, *Computer Vision – ECCV 2014*, pages 48–64, Cham, 2014. Springer International Publishing.

[15] Ankit Dhall, Anastasia Makarova, Octavian Ganea, Dario Pavllo, Michael Greeff, and Andreas Krause. Hierarchical image classification using entailment cone embeddings. In *Proceedings of the IEEE/CVF conference on computer vision and pattern recognition workshops*, pages 836–837, 2020.

[16] Bhuwan Dhingra, Christopher J Shallue, Mohammad Norouzi, Andrew M Dai, and George E Dahl. Embedding text in hyperbolic spaces. *arXiv preprint arXiv:1806.04313*, 2018.

[17] Gamaleldin Elsayed, Dilip Krishnan, Hossein Mobahi, Kevin Regan, and Samy Bengio. Large margin deep networks for classification. *Advances in neural information processing systems*, 31, 2018.

[18] Aleksandr Ermolov, Leyla Mirvakhabova, Valentin Khrulkov, Nicu Sebe, and Ivan Oseledets. Hyperbolic vision transformers: Combining improvements in metric learning. In *Proceedings of the IEEE/CVF Conference on Computer Vision and Pattern Recognition*, pages 7409–7419, 2022.

[19] Christiane Fellbaum. *WordNet: An Electronic Lexical Database*. Bradford Books, 1998.

[20] Octavian Ganea, Gary Bécigneul, and Thomas Hofmann. Hyperbolic neural networks. In *Advances in Neural Information Processing Systems*, pages 5345–5355, 2018.

[21] Songwei Ge, Shlok Mishra, Simon Kornblith, Chun-Liang Li, and David Jacobs. Hyperbolic contrastive learning for visual representations beyond objects. *arXiv preprint arXiv:2212.00653*, 2022.

[22] Robert Geirhos, Patricia Rubisch, Claudio Michaelis, Matthias Bethge, Felix A. Wichmann, and Wieland Brendel. Imagenet-trained CNNs are biased towards texture; increasing shape bias improves accuracy and robustness. In *International Conference on Learning Representations*, 2019.

[23] Mikhael Gromov. Hyperbolic groups. In *Essays in group theory*, pages 75–263. Springer, 1987.

[24] Caglar Gulcehre, Misha Denil, Mateusz Malinowski, Ali Razavi, Razvan Pascanu, Karl Moritz Hermann, Peter Battaglia, Victor Bapst, David Raposo, Adam Santoro, et al. Hyperbolic attention networks. *arXiv preprint arXiv:1805.09786*, 2018.

[25] Yanming Guo, Yu Liu, Erwin M Bakker, Yuanhao Guo, and Michael S Lew. Cnn-rnn: a large-scale hierarchical image classification framework. *Multimedia tools and applications*, 77(8):10251–10271, 2018.

[26] Yunhui Guo, Xudong Wang, Yubei Chen, and Stella X Yu. Clipped hyperbolic classifiers are super-hyperbolic classifiers. In *Proceedings of the IEEE/CVF Conference on Computer Vision and Pattern Recognition*, pages 11–20, 2022.

[27] Kaiming He, Haoqi Fan, Yuxin Wu, Saining Xie, and Ross Girshick. Momentum contrast for unsupervised visual representation learning. In *Proceedings of the IEEE/CVF conference on computer vision and pattern recognition*, pages 9729–9738, 2020.

[28] Kaiming He, Xiangyu Zhang, Shaoqing Ren, and Jian Sun. Deep residual learning for image recognition, 2015.

[29] Olivier Henaff. Data-efficient image recognition with contrastive predictive coding. In *International conference on machine learning*, pages 4182–4192. PMLR, 2020.

[30] Dan Hendrycks and Kevin Gimpel. A baseline for detecting misclassified and out-of-distribution examples in neural networks. In *5th International Conference on Learning Representations, ICLR 2017*, 2017.

[31] Dan Hendrycks, Mantas Mazeika, and Thomas Dietterich. Deep anomaly detection with outlier exposure. In *ICLR*, 2019.

[32] Dan Hendrycks, Norman Mu, Ekin D. Cubuk, Barret Zoph, Justin Gilmer, and Balaji Lakshminarayanan. AugMix: A simple data processing method to improve robustness and uncertainty. *Proceedings of the International Conference on Learning Representations (ICLR)*, 2020.

[33] R Devon Hjelm, Alex Fedorov, Samuel Lavoie-Marchildon, Karan Grewal, Phil Bachman, Adam Trischler, and Yoshua Bengio. Learning deep representations by mutual information estimation and maximization. *arXiv preprint arXiv:1808.06670*, 2018.

[34] David T Hoffmann, Nadine Behrmann, Juergen Gall, Thomas Brox, and Mehdi Noroozi. Ranking info noise contrastive estimation: Boosting contrastive learning via ranked positives. In *AAAI Conference on Artificial Intelligence*, 2022.

[35] Roger A. Horn and Charles R. Johnson. *Matrix analysis*. Cambridge University Press, Cambridge; New York, 2nd ed edition, 2012.

[36] Yen-Chang Hsu, Yilin Shen, Hongxia Jin, and Zsolt Kira. Generalized odin: Detecting out-of-distribution image without learning from out-of-distribution data. In *Proceedings of the IEEE/CVF Conference on Computer Vision and Pattern Recognition*, pages 10951–10960, 2020.

[37] Rui Huang and Yixuan Li. Towards scaling out-of-distribution detection for large semantic space. *Proceedings of the IEEE/CVF Conference on Computer Vision and Pattern Recognition*, 2021.

[38] Edmond Jonckheere, Poonsuk Lohsoonthorn, and Francis Bonahon. Scaled gromov hyperbolic graphs. *Journal of Graph Theory*, 57(2):157–180, 2008.

[39] Prannay Khosla, Piotr Teterwak, Chen Wang, Aaron Sarna, Yonglong Tian, Phillip Isola, Aaron Maschinot, Ce Liu, and Dilip Krishnan. Supervised contrastive learning. In *Advances in Neural Information Processing Systems*, volume 33, pages 18661–18673, 2020.

[40] Valentin Khrulkov, Leyla Mirvakhabova, Evgeniya Ustinova, Ivan Oseledets, and Victor Lempitsky. Hyperbolic image embeddings. In *Proceedings of the IEEE/CVF Conference on Computer Vision and Pattern Recognition*, pages 6418–6428, 2020.

[41] Sungyeon Kim, Dongwon Kim, Minsu Cho, and Suha Kwak. Proxy anchor loss for deep metric learning. In *Proceedings of the IEEE/CVF conference on computer vision and pattern recognition*, pages 3238–3247, 2020.

[42] Polina Kirichenko, Pavel Izmailov, and Andrew G Wilson. Why normalizing flows fail to detect out-of-distribution data. *Advances in Neural Information Processing Systems*, 33, 2020.

[43] Alexander Kolesnikov, Lucas Beyer, Xiaohua Zhai, Joan Puigcerver, Jessica Yung, Sylvain Gelly, and Neil Houlsby. Large scale learning of general visual representations for transfer. *arXiv preprint arXiv:1912.11370*, 2(8), 2019.

[44] Dmitri Krioukov, Fragkiskos Papadopoulos, Maksim Kitsak, Amin Vahdat, and Marián Boguná. Hyperbolic geometry of complex networks. *Physical Review E*, 82(3):036106, 2010.

[45] Alex Krizhevsky, Geoffrey Hinton, et al. Learning multiple layers of features from tiny images. 2009.

[46] Christopher Lang, Alexander Braun, Lars Schillingmann, and Abhinav Valada. On hyperbolic embeddings in object detection. In *Pattern Recognition: 44th DAGM German Conference, DAGM GCPR 2022, Konstanz, Germany, September 27–30, 2022, Proceedings*, pages 462–476. Springer, 2022.

[47] Kimin Lee, Kibok Lee, Honglak Lee, and Jinwoo Shin. A simple unified framework for detecting out-of-distribution samples and adversarial attacks. In *Advances in Neural Information Processing Systems*, pages 7167–7177, 2018.

[48] Jie Lei, Zhenyu Guo, and Yang Wang. Weakly supervised image classification with coarse and fine labels. In *2017 14th Conference on Computer and Robot Vision (CRV)*, pages 240–247. IEEE, 2017.

[49] Li-Jia Li, Chong Wang, Yongwhan Lim, David M. Blei, and Li Fei-Fei. Building and using a semantivisual image hierarchy. In *2010 IEEE Computer Society Conference on Computer Vision and Pattern Recognition*, pages 3336–3343, 2010.

[50] Lingxiao Li, Yi Zhang, and Shuhui Wang. The euclidean space is evil: hyperbolic attribute editing for few-shot image generation. In *Proceedings of the IEEE/CVF International Conference on Computer Vision*, pages 22714–22724, 2023.

[51] Shiyu Liang, Yixuan Li, and R. Srikant. Enhancing the reliability of out-of-distribution image detection in neural networks. In *6th International Conference on Learning Representations, ICLR 2018*, 2018.

[52] Shaoteng Liu, Jingjing Chen, Liangming Pan, Chong-Wah Ngo, Tat-Seng Chua, and Yu-Gang Jiang. Hyperbolic visual embedding learning for zero-shot recognition. In *Proceedings of the IEEE/CVF conference on computer vision and pattern recognition*, pages 9273–9281, 2020.

[53] Weitang Liu, Xiaoyun Wang, John Owens, and Yixuan Li. Energy-based out-of-distribution detection. *Advances in Neural Information Processing Systems*, 2020.

[54] Weiyang Liu, Yandong Wen, Zhiding Yu, and Meng Yang. Large-margin softmax loss for convolutional neural networks. *arXiv preprint arXiv:1612.02295*, 2016.

[55] Teng Long, Pascal Mettes, Heng Tao Shen, and Cees G. M. Snoek. Searching for actions on the hyperbole. In *Proceedings of the IEEE/CVF Conference on Computer Vision and Pattern Recognition (CVPR)*, June 2020.

[56] Emile Mathieu, Charline Le Lan, Chris J Maddison, Ryota Tomioka, and Yee Whye Teh. Continuous hierarchical representations with poincaré variational auto-encoders. *Advances in neural information processing systems*, 32, 2019.

[57] Leland McInnes, John Healy, and James Melville. Umap: Uniform manifold approximation and projection for dimension reduction. *arXiv preprint arXiv:1802.03426*, 2018.

[58] I. McLean, A.B. Urken, and F. Hewitt. *Classics of social choice*. University of Michigan Press, 1995. Citation Key: mclean1995classics tex.lccn: 94024390.

[59] Yifei Ming, Ziyang Cai, Jiuxiang Gu, Yiyou Sun, Wei Li, and Yixuan Li. Delving into out-of-distribution detection with vision-language representations. In *Advances in Neural Information Processing Systems*, 2022.

[60] Yifei Ming, Ying Fan, and Yixuan Li. POEM: Out-of-distribution detection with posterior sampling. In *Proceedings of the 39th International Conference on Machine Learning*, pages 15650–15665, 2022.

[61] Yifei Ming, Yiyou Sun, Ousmane Dia, and Yixuan Li. How to exploit hyperspherical embeddings for out-of-distribution detection? In *The Eleventh International Conference on Learning Representations*, 2022.

[62] Gal Mishne, Zhengchao Wan, Yusu Wang, and Sheng Yang. The numerical stability of hyperbolic representation learning. In *International Conference on Machine Learning*, pages 24925–24949. PMLR, 2023.

[63] Eric Nalisnick, Akihiro Matsukawa, Yee Whye Teh, Dilan Gorur, and Balaji Lakshminarayanan. Do deep generative models know what they don't know? In *International Conference on Learning Representations*, 2019.

[64] Nelson Nauata, Hexiang Hu, Guang-Tong Zhou, Zhiwei Deng, Zicheng Liao, and Greg Mori. Structured label inference for visual understanding. *IEEE transactions on pattern analysis and machine intelligence*, 42(5):1257–1271, 2019.

[65] Yuval Netzer, Tao Wang, Adam Coates, Alessandro Bissacco, Bo Wu, and Andrew Y Ng. Reading digits in natural images with unsupervised feature learning. 2011.

[66] Maximillian Nickel and Douwe Kiela. Poincaré embeddings for learning hierarchical representations. In *Advances in Neural Information Processing Systems*, pages 6338–6347, 2017.

[67] Maximillian Nickel and Douwe Kiela. Learning continuous hierarchies in the Lorentz model of hyperbolic geometry. In Jennifer Dy and Andreas Krause, editors, *Proceedings of the 35th International Conference on Machine Learning*, volume 80 of *Proceedings of Machine Learning Research*, pages 3779–3788. PMLR, 10–15 Jul 2018.

[68] Khondaker Tasrif Noor, Antonio Robles-Kelly, and Brano Kusy. A capsule network for hierarchical multi-label image classification. In *Joint IAPR International Workshops on Statistical Techniques in Pattern Recognition (SPR) and Structural and Syntactic Pattern Recognition (SSPR)*, pages 163–172. Springer, 2022.

[69] Francesco Pinto, Harry Yang, Ser-Nam Lim, Philip Torr, and Puneet K. Dokania. Using mixup as a regularizer can surprisingly improve accuracy & out-of-distribution robustness. In Alice H. Oh, Alekh Agarwal, Danielle Belgrave, and Kyunghyun Cho, editors, *Advances in Neural Information Processing Systems*, 2022.

[70] Erzsébet Ravasz and Albert-László Barabási. Hierarchical organization in complex networks. *Physical review E*, 67(2):026112, 2003.

[71] Jie Ren, Peter J Liu, Emily Fertig, Jasper Snoek, Ryan Poplin, Mark Depristo, Joshua Dillon, and Balaji Lakshminarayanan. Likelihood ratios for out-of-distribution detection. In *Advances in Neural Information Processing Systems*, pages 14680–14691, 2019.

[72] Olga Russakovsky, Jia Deng, Hao Su, Jonathan Krause, Sanjeev Satheesh, Sean Ma, Zhiheng Huang, Andrej Karpathy, Aditya Khosla, Michael Bernstein, Alexander C. Berg, and Li Fei-Fei. ImageNet Large Scale Visual Recognition Challenge. *International Journal of Computer Vision (IJCV)*, 115(3):211–252, 2015.

[73] Frederic Sala, Chris De Sa, Albert Gu, and Christopher Ré. Representation tradeoffs for hyperbolic embeddings. In *Proceedings of the International Conference on Machine Learning*, pages 4460–4469, 2018.

[74] Shibani Santurkar, Dimitris Tsipras, and Aleksander Madry. Breeds: Benchmarks for subpopulation shift. In *International Conference on Learning Representations*, 2021.

[75] Rik Sarkar. *Low Distortion Delaunay Embedding of Trees in Hyperbolic Plane*, volume 7034 of *Lecture Notes in Computer Science*, page 355–366. Springer Berlin Heidelberg, Berlin, Heidelberg, 2012.

[76] Vikash Sehwag, Mung Chiang, and Prateek Mittal. Ssd: A unified framework for self-supervised outlier detection. In *International Conference on Learning Representations*, 2021.

[77] Joan Serrà, David Álvarez, Vicenç Gómez, Olga Slizovskaia, José F. Núñez, and Jordi Luque. Input complexity and out-of-distribution detection with likelihood-based generative models. In *International Conference on Learning Representations*, 2020.

[78] Ryohei Shimizu, Yusuke Mukuta, and Tatsuya Harada. Hyperbolic neural networks++. In *International Conference on Learning Representations*, 2020.

[79] Robert R. Sokal and F. James Rohlf. The comparison of dendrograms by objective methods. *Taxon*, 1962.

[80] Yue Song, Nicu Sebe, and Wei Wang. Rankfeat: Rank-1 feature removal for out-of-distribution detection. In Alice H. Oh, Alekh Agarwal, Danielle Belgrave, and Kyunghyun Cho, editors, *Advances in Neural Information Processing Systems*, 2022.

[81] Sainbayar Sukhbaatar, Joan Bruna, Manohar Paluri, Lubomir Bourdev, and Rob Fergus. Training convolutional networks with noisy labels. *arXiv preprint arXiv:1406.2080*, 2014.

[82] Yiyou Sun, Chuan Guo, and Yixuan Li. React: Out-of-distribution detection with rectified activations. In *Advances in Neural Information Processing Systems*, 2021.

[83] Yiyou Sun, Yifei Ming, Xiaojin Zhu, and Yixuan Li. Out-of-distribution detection with deep nearest neighbors. *ICML*, 2022.

[84] Atsushi Suzuki, Atsushi Nitanda, Jing Wang, Linchuan Xu, Kenji Yamanishi, and Marc Cavazza. Generalization error bound for hyperbolic ordinal embedding. In *International Conference on Machine Learning*, pages 10011–10021. PMLR, 2021.

[85] Jihoon Tack, Sangwoo Mo, Jongheon Jeong, and Jinwoo Shin. Csi: Novelty detection via contrastive learning on distributionally shifted instances. In *Advances in Neural Information Processing Systems*, 2020.

[86] Fariborz Taherkhani, Hadi Kazemi, Ali Dabouei, Jeremy Dawson, and Nasser M Nasrabadi. A weakly supervised fine label classifier enhanced by coarse supervision. In *Proceedings of the IEEE/CVF International Conference on Computer Vision*, pages 6459–6468, 2019.

[87] Yonglong Tian, Dilip Krishnan, and Phillip Isola. Contrastive multiview coding. In *Computer Vision–ECCV 2020: 16th European Conference, Glasgow, UK, August 23–28, 2020, Proceedings, Part XI 16*, pages 776–794. Springer, 2020.

[88] Abraham A Ungar. Hyperbolic trigonometry and its application in the poincaré ball model of hyperbolic geometry. *Computers & Mathematics with Applications*, 41(1-2):135–147, 2001.

[89] Laurens Van der Maaten and Geoffrey Hinton. Visualizing data using t-sne. *Journal of machine learning research*, 9(11), 2008.

[90] Grant Van Horn, Oisin Mac Aodha, Yang Song, Yin Cui, Chen Sun, Alex Shepard, Hartwig Adam, Pietro Perona, and Serge Belongie. The inaturalist species classification and detection dataset. In *Proceedings of the IEEE Conference on Computer Vision and Pattern Recognition (CVPR)*, June 2018.

[91] Panqu Wang and Garrison W. Cottrell. Basic level categorization facilitates visual object recognition, 2015.

[92] Hongxin Wei, Renchunzi Xie, Hao Cheng, Lei Feng, Bo An, and Yixuan Li. Mitigating neural network overconfidence with logit normalization. In *ICML*, 2022.

[93] Hermann Weyl. Das asymptotische verteilungsgesetz der eigenwerte linearer partieller differentialgleichungen (mit einer anwendung auf die theorie der hohlraumstrahlung). *Mathematische Annalen*, 71(4):441–479, December 1912.

[94] Jim Winkens, Rudy Bunel, Abhijit Guha Roy, Robert Stanforth, Vivek Natarajan, Joseph R Ledsam, Patricia MacWilliams, Pushmeet Kohli, Alan Karthikesalingam, Simon Kohl, et al. Contrastive training for improved out-of-distribution detection. *arXiv preprint arXiv:2007.05566*, 2020.

[95] Zhirong Wu, Yuanjun Xiong, Stella X Yu, and Dahua Lin. Unsupervised feature learning via non-parametric instance discrimination. In *Proceedings of the IEEE conference on computer vision and pattern recognition*, pages 3733–3742, 2018.

[96] Jianxiong Xiao, James Hays, Krista A Ehinger, Aude Oliva, and Antonio Torralba. Sun database: Large-scale scene recognition from abbey to zoo. In *2010 IEEE computer society conference on computer vision and pattern recognition*, pages 3485–3492. IEEE, 2010.

[97] Zhisheng Xiao, Qing Yan, and Yali Amit. Likelihood regret: An out-of-distribution detection score for variational auto-encoder. *Advances in Neural Information Processing Systems*, 33, 2020.

[98] Qizhe Xie, Minh-Thang Luong, Eduard Hovy, and Quoc V Le. Self-training with noisy student improves imagenet classification. In *Proceedings of the IEEE/CVF conference on computer vision and pattern recognition*, pages 10687–10698, 2020.

[99] Pingmei Xu, Krista A Ehinger, Yinda Zhang, Adam Finkelstein, Sanjeev R Kulkarni, and Jianxiong Xiao. Turkergaze: Crowdsourcing saliency with webcam based eye tracking. *arXiv preprint arXiv:1504.06755*, 2015.

[100] Jiexi Yan, Lei Luo, Cheng Deng, and Heng Huang. Unsupervised hyperbolic metric learning. In *Proceedings of the IEEE/CVF Conference on Computer Vision and Pattern Recognition*, pages 12465–12474, 2021.

[101] Zhicheng Yan, Hao Zhang, Robinson Piramuthu, Vignesh Jagadeesh, Dennis DeCoste, Wei Di, and Yizhou Yu. Hd-cnn: Hierarchical deep convolutional neural network for large scale visual recognition, 2014.

[102] Fisher Yu, Ari Seff, Yinda Zhang, Shuran Song, Thomas Funkhouser, and Jianxiong Xiao. Lsun: Construction of a large-scale image dataset using deep learning with humans in the loop. *arXiv preprint arXiv:1506.03365*, 2015.

[103] Yun Yue, Fangzhou Lin, Kazunori D Yamada, and Ziming Zhang. Hyperbolic contrastive learning. *arXiv preprint arXiv:2302.01409*, 2023.

[104] Siqi Zeng, Remi Tachet des Combes, and Han Zhao. Learning structured representations by embedding class hierarchy. In *The Eleventh International Conference on Learning Representations*, 2022.

[105] Jingyang Zhang, Nathan Inkawhich, Randolph Linderman, Yiran Chen, and Hai Li. Mixture outlier exposure: Towards out-of-distribution detection in fine-grained environments. In *Proceedings of the IEEE/CVF Winter Conference on Applications of Computer Vision (WACV)*, pages 5531–5540, January 2023.

[106] Jingyang Zhang, Jingkang Yang, Pengyun Wang, Haoqi Wang, Yueqian Lin, Haoran Zhang, Yiyou Sun, Xuefeng Du, Kaiyang Zhou, Wayne Zhang, et al. Openood v1. 5: Enhanced benchmark for out-of-distribution detection. *arXiv preprint arXiv:2306.09301*, 2023.

[107] Zhilu Zhang and Mert Sabuncu. Generalized cross entropy loss for training deep neural networks with noisy labels. *Advances in neural information processing systems*, 31, 2018.

[108] Yu Zheng, Jianping Fan, Ji Zhang, and Xinbo Gao. Hierarchical learning of multi-task sparse metrics for large-scale image classification. *Pattern Recognition*, 67:97–109, 2017.

[109] Bolei Zhou, Agata Lapedriza, Aditya Khosla, Aude Oliva, and Antonio Torralba. Places: A 10 million image database for scene recognition. *IEEE transactions on pattern analysis and machine intelligence*, 40(6):1452–1464, 2017.

[110] Chengxu Zhuang, Alex Lin Zhai, and Daniel Yamins. Local aggregation for unsupervised learning of visual embeddings. In *Proceedings of the IEEE/CVF international conference on computer vision*, pages 6002–6012, 2019.

Appendix

This appendix is segmented into the following key parts.

1. **Section A** continues the analysis of the eigenspectrum of CPCC-optimized representation matrix and generalizes it for an arbitrary label tree.
2. **Section B** discusses additional details about our proposed method `HypStructure`, its implementation and broader impact of our work. In particular, an overview of the method is first provided, and then we describe hyperparameter settings of our method and the main baselines, followed by extra dataset details and explanation of evaluation metrics.
3. **Section C** reports ablation studies, detailed results on OOD detection and provides additional experimental results and visualizations not included in the main paper due to lack of space.

A Details of Eigenspectrum Analysis

In this section, we first introduce some notations, discuss the setup for our analysis, followed by preliminary lemmas, and then characterize the eigenspectrum of CPCC-based structured representations in Theorem A.2 for an arbitrary label tree and Theorem 5.1 for a balanced tree presented in the main body.

Proof Sketch The proof of Theorem A.2 and Theorem 5.1 relies on the important observation of a *hierarchical* block structure of the covariance matrix of CPCC-regularized features, as shown in Figure 8a, which will also be supported by Lemma A.1 and Corollary A.1. Theorem A.1 [3] and Lemma A.2 characterize the eigenvalues of a block correlation matrix induced from a basic tree where the matrix only has three types of values: diagonal values of 1s, one for within group entry, and another for across group entry. Larger within group entries lead to the larger eigenvalues. Theorem A.1 [3] and Lemma A.2 are then used as the base case for the induction proof of Theorem 5.1. For an arbitrary tree, in Theorem A.2, we use Weyl's Theorem [93] to bound the gap between within group entries and across group entries that leads to the phase transition of eigenvalues.

Setup details After training with the `HypStructure` loss till convergence, let us denote the feature matrix as $Z \in \mathbb{R}^{n \times d}$, where each row of Z is a d-dimensional vector of an in distribution training sample, and the CPCC is maximized to 1. We let $C_0 = n, C_1, C_2, \ldots, C_H = 1$ be the number of class labels at height h of the tree $\mathcal{T}$. Following the standard pre-processing steps in OOD detection [76], we assume that the features are standardized and normalized so that $\mathbb{E}[Z] = \mathbf{0}$ and $\|Z_i\|_2 = 1, \forall i$. Besides, we assume that in $\mathcal{T}$, the distance from root node to each leaf node is the same. Otherwise, following [74], we can insert dummy parents or children into the tree to make sure vertices at the same level have similar visual granularity. We then apply CPCC to each node in the extended tree, where each leaf node is one sample. We note that although this is slightly different from the implementation where the leaf nodes are fine class nodes, the distance for samples within fine classes are automatically minimized by classification loss like cross-entropy and supervised contrastive loss.

Given these assumptions, we want to analyze the eigenspectrum of the inverse sample covariance matrix $\frac{1}{n-1}Z^\top Z$, which is the same as investigating the eigenvalues of $K = ZZ^\top$ where Z is ordered by classes at all levels, i.e., samples having the same fine-grained labels and coarse labels should be placed together. This is because the matrix scaling and permutation will not change the order of singular values.

Since CPCC (eq. (1)) is a correlation coefficient, when it is maximized, the n by n pairwise Poincaré distance matrix is perfectly correlated with the ground truth pairwise *tree-metric* matrix, where each entry is the tree distance between two samples on the tree, no matter we apply CPCC to leaves or all vertices. This implies that in the similarity matrix K, the relative order of entries are the opposite of tree matrix, and it is trivial to show it as follows

Lemma A.1. The relative order of entries in K will be the reverse of the order in tree distance.

Proof. When $\|u\| = \|v\| = 1$, $\ell_2(u,v)^2 = \|u - v\|_2^2 = \|u\|^2 + \|v\|^2 - 2\langle u, v\rangle = 2 - 2\langle u, v\rangle$. Now considering the CPCC computation, if the CPCC is maximized, the pairwise Euclidean matrix is of the scalar factor of the tree distance matrix. Since each entry of K is the dot product of two samples, the relative order in K is the opposite. ■

Corollary A.1. If we use the Poincaré distance (eq. (3) in CPCC and let the curvature constant $c = 1$, the statement of cosine distance in Lemma A.1 still holds.

Proof. Since the Poincaré distance (eq. (3)) is only defined for vectors with magnitude less than 1, let us consider the case where before the clipping operation, both u and v are outside the unit ball. After applying clip[1], $\|u\| = \|v\| = 1 - \epsilon$, where ϵ is a small constant (10^-5). Then $\|u\|^2 = (1-\epsilon)^2 = 1 - 2\epsilon + \epsilon^2$. Define $2\epsilon - \epsilon^2$ as ξ, making $\|u\|^2 := 1 - \xi$ where ξ is also a small constant such that $O(\xi^2)$ is negligible.

$$
\begin{aligned}
\text{Poincaré}(u, v) &= 2 \ln \frac{\|u - v\| + \sqrt{\|u\|^2 \|v\|^2 - 2u \cdot v + 1}}{\sqrt{(1 - \|u\|^2)(1 - \|v\|^2)}} \\
&= 2 \ln \frac{\|u - v\| + \sqrt{2 - 2u \cdot v - 2\xi + \xi^2}}{\xi} \\
&\approx 2 \ln \frac{\|u - v\| + \sqrt{2 - 2u \cdot v - 2\xi}}{\xi} \\
&= 2 \ln \frac{\|u - v\| + \sqrt{\|u\|^2 + \|v\|^2 - 2u \cdot v}}{\xi} \\
&= 2 \ln \frac{2\,\|u - v\|}{\xi}
\end{aligned}
$$

We can see that the Poincaré distance monotonically increases with Euclidean distances $\|u - v\|$. This property ensures the relative order of any two entries for Euclidean CPCC and Poincare CPCC matrices in K to be the same. Then, we can argue about the structure of K, either Euclidean or Poincare, to have the hierarchical diagonalized structure as in Figure 8a. So any statement applied for a Poincaré version of CPCC will also hold for the Euclidean CPCC counterpart. ■

For each level of the tree, due to the optimization of CPCC loss, the corresponding off diagonal entries of K, which represent the intra-level-class similarities, are much smaller than inter-level-class values. We thus have a symmetric similarity matrix that takes on the following structure, where the red regions are greater than orange regions, which are further greater than the blue regions.

$$
K = \left[\begin{array}{cc:cc:cc:cc:c}
1 & r^1_{11} & r^2_{12} & r^2_{12} & r^3_{13} & r^3_{13} & r^3_{14} & r^3_{14} & \cdots \\
r^1_{11} & 1 & r^2_{12} & r^2_{12} & r^3_{13} & r^3_{13} & r^3_{14} & r^3_{14} & \cdots \\
\hdashline
r^2_{12} & r^2_{12} & 1 & r^1_{22} & r^3_{23} & r^3_{23} & r^3_{24} & r^3_{24} & \cdots \\
r^2_{12} & r^2_{12} & r^1_{22} & 1 & r^3_{23} & r^3_{23} & r^3_{24} & r^3_{24} & \cdots \\
\hdashline
r^3_{13} & r^3_{13} & r^3_{23} & r^3_{23} & 1 & r^1_{33} & r^2_{34} & r^2_{34} & \cdots \\
r^3_{13} & r^3_{13} & r^3_{23} & r^3_{23} & r^1_{33} & 1 & r^2_{34} & r^2_{34} & \cdots \\
\hdashline
r^3_{14} & r^3_{14} & r^3_{24} & r^3_{24} & r^2_{34} & r^2_{34} & 1 & r^1_{44} & \cdots \\
r^3_{14} & r^3_{14} & r^3_{24} & r^3_{24} & r^2_{34} & r^2_{34} & r^1_{44} & 1 & \cdots \\
\hdashline
\cdots & \cdots & \cdots & \cdots & \cdots & \cdots & \cdots & \cdots & \cdots
\end{array}\right]
$$

Each non-diagonal entry is called r^h_{ij} where i, j are the index of the diagonal block, or the *finest* label id of one sample, and h is the height of the lowest common ancestor of the two samples in the row and the column. Since every two leaves sharing the lowest common ancestor of the same height have the same tree distance, each entry of K with the same superscript will be the same so we can drop the i, j subscript in the notation. The size of each block is defined by the number of samples within one label. Then, the shown submatrix of K corresponds to the following tree in Figure 9. Next, we present several useful lemmas and theorems.

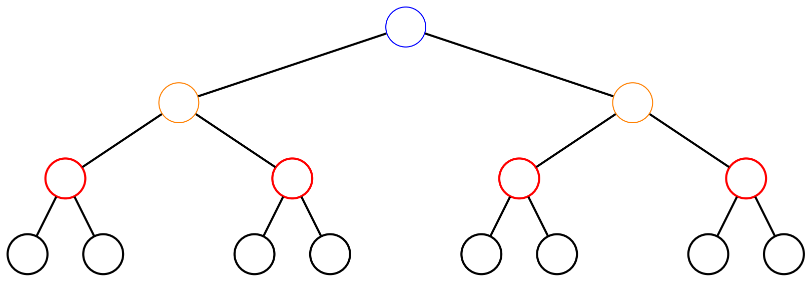
Figure 9: Subtree corresponds to the shown submatrix of K.

Theorem A.1 ([3])**.** Let R be a $p \times p$ full-rank correlation matrix that has a k-group block structure, with groups of size p_i ($i = 1 : k$, $\sum_{i=1}^{k} p_i = p$). Let r_{ii} be the correlation for any pair of different variables within group i. Let r_{ij} be the common correlation between any variable in group i and j. Denote the mean of the i-th diagonal block of R by $\overline{R_i} = (1/p_i)(1 + (p_i - 1)r_{ii})$. Then:

1. R has $p_i - 1$ eigenvalues $1 - r_{ii}$ ($i = 1 : k$).
2. The rest of the eigenvalues are those from $k \times k$ symmetric matrix A whose diagonal elements are $a_{ii} = p_i\overline{R_i}$ and whose off-diagonal elements are $a_{ij} = \sqrt{p_i \cdot p_j} r_{ij}$.

Lemma A.2. Given d by d matrix M where $M_{ii} = 1, \forall i \in [d]$, and $M_{ij} = p$ otherwise, i.e.,

$$M = \begin{bmatrix} 1 & p & \dots & \dots & p \\ p & \ddots & & & \vdots \\ \vdots & & 1 & & \vdots \\ \vdots & & & \ddots & p \\ p & \dots & \dots & p & 1 \end{bmatrix}$$

it has eigenvalues $\lambda_1 = 1 + p(d-1)$ and $\lambda_2 = \dots = \lambda_d = 1 - p$.

Proof. Using the definition of eigenvalues, we want to compute the determinant of matrix

$$\begin{bmatrix} 1-\lambda & p & \dots & \dots & p \\ p & \ddots & & & \vdots \\ \vdots & & 1-\lambda & & \vdots \\ \vdots & & & \ddots & p \\ p & \dots & \dots & p & 1-\lambda \end{bmatrix}$$

Adding the second till the last row to the first row, we have

$$\begin{bmatrix} 1-\lambda+(d-1)p & 1-\lambda+(d-1)p & \dots & \dots & 1-\lambda+(d-1)p \\ p & \ddots & & & \vdots \\ \vdots & & 1-\lambda & & \vdots \\ \vdots & & & \ddots & p \\ p & \dots & \dots & p & 1-\lambda \end{bmatrix}$$

Dividing the first row by $1 - \lambda + (d-1)p$, we now have

$$\begin{bmatrix} 1 & 1 & \dots & \dots & 1 \\ p & \ddots & & & \vdots \\ \vdots & & 1-\lambda & & \vdots \\ \vdots & & & \ddots & p \\ p & \dots & \dots & p & 1-\lambda \end{bmatrix}$$

Subtracting the second till the last row by p times the first row results in an upper triangular matrix

$$\begin{bmatrix} 1 & 1 & \dots & \dots & 1 \\ 0 & 1-\lambda-p & & & 0 \\ \vdots & & 1-\lambda-p & & \vdots \\ \vdots & & & \ddots & 0 \\ 0 & \dots & \dots & 0 & 1-\lambda-p \end{bmatrix}$$

Thus, $\det(M-\lambda I) = (1-\lambda+(d-1)p)(1-\lambda-p)^{d-1}$. ∎

Notice that Lemma A.2 is a special case of Theorem A.1 where the label tree is a two level basic tree with the root node and d leaves in the second label all being the direct children of the root node. Now we can leverage Theorem A.1 and Lemma A.2 to investigate the eigenspectrum of K by proving the following theorem:

Theorem A.2 (**Eigenspectrum of CPCC-based Structured Representation**)**.** If $\mathcal{T}$ is a tree whose root node has height H where each level has C_h nodes, $h \in [0, H]$. $K = Z^\top Z$ is a block structured correlation matrix as a result of CPCC optimization, where each off-diagonal entry $\in [-1,1]$ can be written as r^h and h is the height of the lowest common ancestor of the i-th row and the $00j$-th column sample. Let $\Delta = r^1 - r^h$, $p_i, i \in [C_h]$ be the number of children for nodes at height h, and p_{max} be the maximum. For any $h \geq 1$, if $r^h \geq M \geq 0$, $r^{h+1} \leq m$, then

(i) We have $C_0 - C_h$ eigenvalues, that come from the eigenvalues of a $C_0 \times C_0$ matrix sharing the same C_h of $p_i \times p_i$ diagonal blocks from K subtracting r^h, and off diagonal values are all zero.

(ii) The rest of C_h eigenvalues come from a $C_h \times C_h$ matrix, whose diagonal entries are the mean of each $p_i \times p_i$ diagonal block from K, and the off diagonal entries are $\sqrt{p_i p_j} r_{ij}$ where r_{ij} is the correlation between node i and node j of height h.

(iii) If $m \leq \frac{M - 2\Delta(p_{\text{max}}-1)}{p_{\text{max}}(C_h - 1)}$, $C_0 - C_h$ eigenvalues are all smaller than C_h eigenvalues.

Proof. Part (i) and (ii) can be extended from the proof of Theorem A.1. Let G be the $n \times C_h$ matrix where $G_{ij} = 1$ if the i-th sample is in group j, otherwise $G_{ij} = 0$. For any $n - C_h$ eigenvectors in the orthogonal complement of the column space of G, the eigenvector of K is also the eigenvector of

$$\begin{bmatrix} K_1 & \mathbf{0} & \cdots & \mathbf{0} \\ \mathbf{0} & K_2 & \cdots & \mathbf{0} \\ \vdots & \vdots & \ddots & \vdots \\ \mathbf{0} & \mathbf{0} & \cdots & K_k \end{bmatrix}$$

where due to the hierarchical structure of block matrix, K_i has the format of

$$\begin{bmatrix} 1-r^h & r^1-r^h & \cdots & r^j-r^h & 0 & \cdots & 0 \\ r^1-r^h & 1-r^h & \cdots & 0 & 0 & \cdots & 0 \\ \vdots & \vdots & \ddots & \vdots & \vdots & & \vdots \\ r^j-r^h & 0 & \cdots & 1-r^h & 0 & \cdots & 0 \\ 0 & 0 & \cdots & 0 & 1-r^h & \cdots & 0 \\ \vdots & \vdots & & \vdots & \vdots & \ddots & \vdots \\ 0 & 0 & \cdots & 0 & 0 & \cdots & 1-r^h \end{bmatrix}$$

The rest of C_h eigenvectors come from the symmetric $C_h \times C_h$ matrix $A = (G^\top G)^{-1/2}(G^\top K G)(G^\top G)^{-1/2}$, by some basica algebra, we know $a_{ij} = \frac{1}{\sqrt{p_i}} \cdot$ (sum of all r_{ij} entries in $p_i \times p_j$ block) $\cdot \frac{1}{\sqrt{p_j}}$. For more details, we refer the reader to Theorem 3.1 in [3] where $C_1 = k$ using their notation.

Since the largest absolute value of K's eigenvalues, is bounded above by the largest row sum of the absolute values of K [35], first $n - C_h$ eigenvectors are bounded above by $U = \max_i (1 - r^h) + (p_i - 1)(r^1 - r^h) = (1 - r^h) + (p_{\text{max}} - 1)\Delta$.

On the other hand, for the rest of C_h eigenvalues, we analyze matrix A:

$$
\begin{aligned}
A &\le A_1 + A_2 \\
&:= \begin{bmatrix} 1+(p_1-1)r^h & 0 & \cdots & 0 \\ 0 & 1+(p_2-1)r^h & \cdots & 0 \\ \vdots & \vdots & \ddots & \vdots \\ 0 & 0 & \cdots & 1+(p_k-1)r^h \end{bmatrix} \\
&+ \begin{bmatrix} (p_{\text{max}}-1)(r^1-r^h) & p_{\text{max}}m & \cdots & p_{\text{max}}m \\ p_{\text{max}}m & (p_{\text{max}}-1)(r^1-r^h) & \cdots & p_{\text{max}}m \\ \vdots & \vdots & \ddots & \vdots \\ p_{\text{max}}m & p_{\text{max}}m & \cdots & (p_{\text{max}}-1)(r^1-r^h) \end{bmatrix}
\end{aligned}
$$

The inequality comes from the effect of the maximization of CPCC that $r^1 \ge \cdots r^h \ge r^{h+1} \ge \cdots r^H$ and $r^h \le m$. The eigenvalues of A_1, A_2 have the analytical form, where A_1's eigenvalues have the form of $1+(p_i-1)r^h$ and A_2's eigenvalues can be derived by Lemma A.2. By Weyl's inequality [93], the minimum of these C_h eigenvalues is at least $L = (1+(p_{\text{min}}-1)r^h) - [(p_{\text{max}}-1)\Delta - p_{\text{max}}m + kp_{\text{max}}m] \ge (1+(1-1)r^h) - [(p_{\text{max}}-1)\Delta - p_{\text{max}}m + kp_{\text{max}}m]$.

To guarantee eigenvalues from Part (ii) are larger, we want $L \ge U$. We solve this inequality with m, and we will get the desired range of m. ■

When $r^h = r^1$ in Theorem A.2, we have $\Delta = 0$. Therefore, for a three level basic tree with only r^1, r^2, if $m \le M/(p_{\text{max}}(C_1-1))$, $C_0 - C_1$ eigenvalues are all smaller than C_1 eigenvalues. In general, we have shown that when m, i.e., the across group similarity is sufficiently small, the eigenvalue gap always exists. When the label tree $\mathcal{T}$ is balanced, we can further specify the expression of each eigenvalue and the amount of eigenvalue gaps.

We now formally restate the Theorem 4.1 from the main paper and give its proof.

Theorem 5.1 (Eigenspectrum of Structured Representation with Balanced Label Tree). *Let $\mathcal{T}$ be a balanced tree with height H, such that each level has C_h nodes, $h \in [0, H]$. Let us denote each entry of K as r^h where h is the height of the lowest common ancestor of the row and the column sample. If $r^h \ge 0, \forall h$, then: (i) For $h = 0$, we have $C_0 - C_1$ eigenvalues $\lambda_0 = 1 - r^1$. (ii) For $0 < h \le H-1$, we have $C_h - C_{h+1}$ eigenvalues $\lambda_h = \lambda_{h-1} + (r^h - r^{h+1})\frac{C_0}{C_h}$. (iii) The last eigenvalue is $\lambda_H = \lambda_{H-1} + C_0 r^H$.*

Proof. From Corollary A.1, we know that $K \in \mathbb{R}^{C_0 \times C_0}$ has a block-wise structure.

Since all statements are presented recursively, we prove the theorem by structural induction on the height of the tree.

The base case is Lemma A.2 with a two level hierarchy tree where only (i) and (iii) are applicable, and $p = r^1, C_0 = d, C_1 = 1$. By Lemma A.2, K has $C_0 - 1$ eigenvalues as $\lambda_0 = 1 - r^1$, and one eigenvalue as $\lambda_1 = 1 + (C_0 - 1)r^1 = (1 - r^1) + r^1/C_0^{-1}$.

Let us now assume that the theorem is true for the balanced tree whose root node is at height $H-1$. Then if we have a tree with height H. We call the resulting matrix K_H.

By the first bullet point of Theorem A.1 we directly get λ_0 from (i). Then by the second bullet point of Theorem A.1, the rest of the eigenvalues are from the symmetric matrix $A_{H-1} \in \mathbb{R}^{C_1 \times C_1}$ whose diagonal elements are $\gamma = 1 + (C_0/C_1 - 1)r^1$ and whose off diagonal elements are $C_0/C_1 \cdot r^j$ for $j \ge 2$.

The key is to observe that A_{H-1} is still a block structured matrix. After A_{H-1} is scaled by γ, the resulting matrix can be also seen as a result of maximizing CPCC where the off diagonal blocks have smaller values.

Applying the hypothesis induction, we then know the expression of eigenvalues for A_{H-1} as

(i) we have $C_1 - C_2$ eigenvalues of the form

$$\begin{aligned}
\lambda_1 &= \gamma(1 - \frac{r^2 C_0/C_1}{\gamma}) \\
&= \gamma - \frac{C_0}{C_1} r^2 \\
&= 1 + (\frac{C_0}{C_1} - 1) r^1 - \frac{C_0}{C_1} r^2 \\
&= 1 - r^1 + \frac{C_0}{C_1}(r^1 - r^2) \\
&= \lambda_0 + \frac{C_0}{C_1}(r^1 - r^2)
\end{aligned}$$

(ii) For $0 < h \leq H - 2$, we have $C_{h+1} - C_{h+2}$ eigenvalues of the form

$$\begin{aligned}
\lambda_{h+1} - \lambda_h &= \gamma \frac{C_0}{C_1} \left(\frac{r^{h+1}}{\gamma} - \frac{r^{h+2}}{\gamma} \right) \frac{C_1}{C_{h+1}} \\
\lambda_{h+1} &= \lambda_h + (r^{h+1} - r^{h+2}) \frac{C_0}{C_{h+1}}
\end{aligned}$$

(iii) The last eigenvalue is

$$\begin{aligned}
\lambda_H - \lambda_{H-1} &= C_1 r^H / \gamma \cdot \frac{C_0}{C_1} \gamma \\
&= C_0 r^H
\end{aligned}$$

Therefore, we proved the theorem by showing the induction step from K_{H-1} to K_H holds. ■

Note that the true symmetric covariance matrix K' might not be having the exact format as K, but it can be seen as a perturbation of K where $\|K' - K\| \leq \epsilon$, ϵ is a small constant. By Weyl's inequality [93], the approximation error of each eigenvalue is bounded by $[\lambda_i - \epsilon, \lambda_i + \epsilon]$.

B Additional Algorithm and Experimental Details

In this section, we first provide an overview of our algorithm, followed by a discussion on the choice of the *flat* loss and additional experimental details about the training and evaluation metrics.

B.1 Broader Impact Statement

Our work proposes `HypStructure`, a structured hyperbolic regularization approach to embed hierarchical information into the learnt representations. This provides significant advancements in understanding and utilizing hierarchical real-world data, particularly for tasks such as representation learning, classification and OOD detection, and we recognize both positive societal impacts and potential risks of this work. The ability to better model hierarchical data in a structured and interpretable fashion is particularly helpful for domains such as AI for science and healthcare, where the learnt representations will be more reflective of the underlying relationships in the domain space. Additionally, the low-dimensional capabilities of hyperbolic geometry can lead to gains in computational efficiency and reduce the carbon footprint in large scale machine learning. However, real-world hierarchical data often incorporates existing biases which may be amplified by structured representation learning, and hence it is important to incorporate fairness constraints to mitigate this risk.

B.2 Pseudocode for `HypStructure`

The training scheme for our `HypStructure` based structured regularization framework is provided in Algorithm 1. At a high level, in `HypStructure`, we optimize a combination of the following two losses: (1) a *hyperbolic CPCC* loss to encourage the representations in the hyperbolic space to correspond with the label hierarchy, (2) a *hyperbolic centering* loss to position the representation corresponding to the root of the node at the centre of the Poincaré ball and the children nodes around it.

Algorithm 1 `HypStructure`: Hyperbolic Structured Representation Learning

```
Input: Batch size $B$, Label tree $\mathcal{T} = (V, E, e)$, Number of epochs $K$, Task Loss formulation $\ell_{\text{Flat}}$,
    Encoder $f_\theta$, Classifier Head $g_w$, Learning Rate $\eta$, Hyperparameters $\alpha, \beta$
 1: Initialize model parameters: $\theta$, $w$
 2: for epoch = $1, 2, \ldots K$ do
 3:     for batch = $1, 2, \ldots, B$ do
 4:         Get image-label pairs: $\{(\boldsymbol{x}_i, y_i)\}_{i=1}^{B}$
 5:         Forward pass to compute the representations: $(\boldsymbol{z}_1 \ldots \boldsymbol{z}_B) \leftarrow (f_\theta(\boldsymbol{x}_1) \ldots (f_\theta(\boldsymbol{x}_B))$
 6:         Compute the Task loss: $\ell_{\text{Flat}}(g_w(\boldsymbol{z}_i), y_i)$
 7:         Get hyperbolic representations using exp. map (eq. (4)): $\tilde{\boldsymbol{z}}_i \leftarrow \exp_{\mathbf{0}}^{c}(\boldsymbol{z}_i)$
 8:         Calculate class prototypes using hyp. Averaging (eq. (6)): $\omega_i \leftarrow \text{HypAve}_K(\tilde{\boldsymbol{z}}_1^v, \ldots \tilde{\boldsymbol{z}}_j^v)$
 9:         Compute pairwise hyp. distances (eq. (3)) $\forall v_i, v_j \in V : \rho(v_i, v_j) \leftarrow d_{\mathbb{B}_c}(\omega_i, \omega_j)$
10:         Get hyp. CPCC loss (eq. (1): HypCPCC$(d_{\mathcal{T}}, \rho)$
11:         Compute hyp. centering loss using (Equation (6)): $\ell_{\text{center}} = \|\text{HypAve}_B(\tilde{\boldsymbol{z}}_1, \ldots, \tilde{\boldsymbol{z}}_B\|)$
12:         Get total loss using Equation (8): $\mathcal{L}(\mathcal{D}_B)$
13:         Compute Gradients for learnable parameters at time $t$: $\mathbf{u_t}(\theta, w) \leftarrow \nabla_{\theta,w}\mathcal{L}(\mathcal{D}_B)$
14:         Refresh the parameters: $(\theta, w)_{t+1} \leftarrow (\theta, w)_t - \frac{\eta}{B}\mathbf{u_t}(\theta, w)$
Output: $(\boldsymbol{z}_1, \ldots \boldsymbol{z}_N); \theta, w$
```

B.3 Choice of Flat loss

We use the Supervised Contrastive [39] (`SupCon`) loss as the first choice for a *flat* loss in our experimentation. Let q_y be the one-hot vector with the y-th index as 1. The Cross Entropy (`CE`) loss, defined between the predictions $g \circ f_\theta(\boldsymbol{x})$ and the labels y, as $\ell_{\text{CE}}(g \circ f(\boldsymbol{x}), y) := -\sum_{i \in [k]} q_i \log(g(f(\boldsymbol{x}))_i)$ has been used quite extensively in large-scale classification problems in the literature [11, 10, 43, 98]. However, several shortcoming of the `CE` loss, such as lack of robustness [81, 107] and poor generalization [17, 54] have been discovered in recent research. Contrastive learning has emerged as a viable alternative to the `CE` loss, to address these shortcomings [7, 95, 29, 87, 33, 27]. The underlying principle for these methods is to *pull* together embeddings for positive pairs and *push* apart the embeddings for negative samples, in the feature space. In the absence of labels, positive samples are created by data augmentations of images and negative samples are randomly chosen from the minibatch. However, when the labels are available, the class information can be leveraged to extend this methodology as a Supervised Contrastive loss (`SupCon`) by *pulling* together embeddings from the same class, and *pushing* apart the embeddings from different classes. This offers a more stable solution for a variety of tasks [39, 76, 83].

Definition B.1 (SupCon Loss)**.** Given a training sample $\boldsymbol{x}_i$, feature encoder $f_\theta(\cdot)$ and a projection head $h(\cdot)$, we denote the normalized feature representations from the projection head as:

$$u_i = \frac{h\left(f_\theta(\boldsymbol{x}_i)\right)}{\|h(f_\theta(\boldsymbol{x}_i))\|_2}, \tag{10}$$

For the N training samples $\{(\boldsymbol{x}_i, y_i)\}_{i=1}^{N}$, we denote the training batch of $2N$ (augmented) pairs as $\{(\tilde{\boldsymbol{x}}_i, \tilde{y}_i)\}_{i=1}^{2N}$ and define the `SupCon` loss as:

$$\ell_{\text{SupCon}} = \frac{1}{2N}\sum_{i=1}^{2N} -\log \frac{\frac{1}{2N_{y_i}-1}\sum_{k=1}^{2N} \mathbb{1}(k \neq i)\mathbb{1}(\tilde{y}_k = \tilde{y}_i)e^{\boldsymbol{u}_i^T \cdot \boldsymbol{u}_k/\tau}}{\sum_{k=1}^{2N} \mathbb{1}(k \neq i)e^{\boldsymbol{u}_i^T \cdot \boldsymbol{u}_k/\tau}}, \tag{11}$$

where N_{y_i} refers to the number of images with label y_i in the batch, τ is the temperature parameter, $\cdot$ refers to the inner product, and $\boldsymbol{u}_i$ and $\boldsymbol{u}_k$ are the normalized feature representations using Equation (10) for $\tilde{\boldsymbol{x}}_i$ and $\tilde{\boldsymbol{x}}_k$ respectively.

While the numerator in the formulation in Equation (11) only considers the samples (and its augmentations) belonging to the same class, the denominator sums over all the negatives as well. Overall, this encourages the network to closely align the feature representations for *all* the samples belonging to the same class, while *pushing* apart the representations of samples across different classes.

We note that our proposed method `HypStructure` is not limited to the choice of euclidean classification losses as ℓ_{Flat} and we report additional results with hyperbolic classification losses in Sections C.8 and C.9 respectively, demonstrating the wide applicability of our approach.

B.4 Implementation Details

B.4.1 Software and Hardware

We implement our method in PyTorch 2.2.2 and run all experiments on a single NVIDIA GeForce RTX-A6000 GPU. The code for our methodology will be open sourced for a wider audience upon acceptance, in the spirit of reproducible research.

B.4.2 Architecture, Hyperparameters and Training

We use the ResNet-18 [28] network as the backbone for CIFAR10, and ResNet-34 as the backbone for CIFAR100 and ImageNet100 datasets. We use a ReLU activated multi layer perceptron with one hidden layer as the projection head $h(.)$ where its hidden layer dimension is the same as input dimension size and the output dimension is 128. We follow the original hyperparameter settings from [39] for training the CIFAR10 and CIFAR100 models from scratch with a temperature $\tau = 0.1$, feature dimension 512, and training for 500 epochs with an initial learning rate of 0.5 with cosine annealing, optimizing using SGD with momentum 0.9 and weight decay 10^{-4}, and a batch size of 512 for all the experiments. For ImageNet100, we finetune the ResNet-34 for 20 epochs following [61] with an initial learning rate of 0.01 and update the weights of the last residual block and the nonlinear projection head, while freezing the parameters in the first three residual blocks. We use the same α values as the regularization parameters for the CPCC loss in Equation (2) (ℓ_2-CPCC) and in Equation (8) (our proposed method `HypStructure`) for a fair comparison and find that the default regularization hyperparameter for the CPCC loss $\alpha = 1.0$ for both ℓ_2-CPCC and `HypStructure` performs well for the experiments on the CIFAR10 and CIFAR100 datasets. We observe that the experiments on the IMAGENET100 dataset benefit from a lower $\alpha = 0.5$. Additionally, we set the hyperparameter for the centering loss in our methodology as $\beta = 0.01$ for all the experiments. We use the default curvature value of $c = 1.0$ for the mapping and distance computations in the Poincaré ball.

B.4.3 Datasets and Hierarchy

We use the following three datasets for our primary experimentation and training in this work

1. **CIFAR10** ([45]). It consists of 50,000 training images and 10,000 test images from 10 different classes.
2. **CIFAR100**([45]). It also consists of 50,000 training images and 10,000 test images, however the images belong to 100 classes. Note that the classes are not identical to the CIFAR10 dataset.
3. **ImageNet100**([72]). This dataset is created as a subset of the large-scale ImageNet dataset following [59]. The original ImageNet dataset consists of 1,000 classes and 1.2 million training images and 50,000 validation images. We construct the ImageNet100 dataset from this original dataset by sampling 100 classes, which results in 128,241 training images and 5000 validation images. We mention the specific classes used for sampling below.

Following [59], we use the below 100 class id's for creating the ImageNet100 subset: n03877845, n03000684, n03110669, n03710721, n02825657, n02113186, n01817953, n04239074, n02002556, n04356056, n03187595, n03355925, n03125729, n02058221, n01580077, n03016953, n02843684, n04371430, n01944390, n03887697, n04037443, n02493793, n01518878, n03840681, n04179913, n01871265, n03866082, n03180011, n01910747, n03388549, n03908714, n01855032, n02134084, n03400231, n04483307, n03721384, n02033041, n01775062, n02808304, n13052670, n01601694, n04136333, n03272562, n03895866, n03995372, n06785654, n02111889, n03447721, n03666591, n04376876, n03929855, n02128757, n02326432, n07614500, n01695060, n02484975, n02105412, n04090263, n03127925, n04550184, n04606251, n02488702, n03404251, n03633091, n02091635, n03457902, n02233338, n02483362, n04461696, n02871525, n01689811, n01498041, n02107312, n01632458, n03394916, n04147183, n04418357, n03218198, n01917289, n02102318, n02088364, n09835506, n02095570, n03982430, n04041544, n04562935, n03933933, n01843065, n02128925, n02480495, n03425413, n03935335, n02971356, n02124075, n07714571, n03133878, n02097130, n02113799, n09399592, n03594945.

In addition to the training and validation images, we also require the label hierarchy for each of these datasets for the CPCC computation in ℓ_2-CPCC and `HypStructure` approaches. For CIFAR100, we use the three-level hierarchy provided with the dataset release[3]. We show this hierarchy in Table 3, where the top-level is the root of the tree.

Table 3: Class Hierarchy of the CIFAR100 Dataset

Coarse Classes	**Fine Classes**
aquatic mammals	beaver, dolphin, otter, seal, whale
fish	aquarium fish, flatfish, ray, shark, trout
flowers	orchids, poppies, roses, sunflowers, tulips
food containers	bottles, bowls, cans, cups, plates
fruit and vegetables	apples, mushrooms, oranges, pears, sweet peppers
household electrical devices	clock, computer keyboard, lamp, telephone, television
household furniture	bed, chair, couch, table, wardrobe
insects	bee, beetle, butterfly, caterpillar, cockroach
large carnivores	bear, leopard, lion, tiger, wolf
large man-made outdoor things	bridge, castle, house, road, skyscraper
large natural outdoor scenes	cloud, forest, mountain, plain, sea
large omnivores and herbivores	camel, cattle, chimpanzee, elephant, kangaroo
medium-sized mammals	fox, porcupine, possum, raccoon, skunk
non-insect invertebrates	crab, lobster, snail, spider, worm
people	baby, boy, girl, man, woman
reptiles	crocodile, dinosaur, lizard, snake, turtle
small mammals	hamster, mouse, rabbit, shrew, squirrel
trees	maple, oak, palm, pine, willow
vehicles 1	bicycle, bus, motorcycle, pickup truck, train
vehicles 2	lawn-mower, rocket, streetcar, tank, tractor

Since no hierarchy is available for the CIFAR10 and ImageNet100 datasets, we construct a hierarchy for CIFAR10 manually, as seen in Figure 2. For ImageNet100, we create a subtree from the WordNet [4] hierarchy, given the 100 aforementioned classes as leaves. We consider the classes which are one level above the leaf nodes in the hierarchy as the coarse classes, following [104].

For the task of OOD detection, we use the following five diverse OOD datasets for CIFAR10 and CIFAR100 as ID datasets, following the literature [83]: `SVHN` [65], `Textures` [9], `Places365` [109], `LSUN` [102] and `iSUN` [99]. When ImageNet100 is used as the ID dataset, we use 4 diverse OOD datasets as the ones in [37], namely subsets of `iNaturalist` [90], `SUN` [96], `Places` [109] and `Textures` [9]. These datasets have been processed so that there is no overlap with the ImageNet classes.

B.5 Delta Hyperbolicity Metrics

We use Gromov's δ_{rel} to evaluate the tree-likeness of the data in Section 4.1, following [40]. For an arbitrary metric space $\mathcal{X}$ with metric d, for any three points $\boldsymbol{x}, \boldsymbol{y}, \boldsymbol{z} \in \mathcal{X}$, we can define the Gromov product as

$$(\boldsymbol{y}, \boldsymbol{z})_{\boldsymbol{x}} = \frac{1}{2}(d(\boldsymbol{x}, \boldsymbol{y}) + d(\boldsymbol{x}, \boldsymbol{z}) - d(\boldsymbol{y}, \boldsymbol{z}))$$

Then, δ-hyperbolicity can be defined as the minimum value of δ such that for any four points $\boldsymbol{x}, \boldsymbol{y}, \boldsymbol{z}, \boldsymbol{w} \in \mathcal{X}$, the following condition holds:

$$(\boldsymbol{x}, \boldsymbol{z})_{\boldsymbol{w}} \geq \min((\boldsymbol{x}, \boldsymbol{y})_{\boldsymbol{w}}, (\boldsymbol{y}, \boldsymbol{z})_{\boldsymbol{w}}) - \delta$$

It can be shown that equivalently, there exists a geometric definition of δ-hyperbolicity. A geodesic triangle in $\mathcal{X}$ is δ-slim if each of its side is contained in the δ-neighbourhood of the union of the other two sides. We define δ-hyperbolicity as the minimum δ that guarantees any triangle in $\mathcal{X}$ is δ-slim. From Figure 10, when the curvature of the surface increases, the geodesic triangle converges to a tree/star graph, and δ gradually reduces to 0.

Following [40], we use the scale-invariant metric $\delta_{rel} = \frac{2\delta}{\text{diam}(\mathcal{X})}$ for evaluation, so that the δ_{rel} is normalized in $[0, 1]$, and the diam$(\cdot)$ is the set diameter or the maximal pairwise distance.

[3]https://www.cs.toronto.edu/ kriz/cifar.html

[4]https://www.nltk.org/howto/wordnet.html

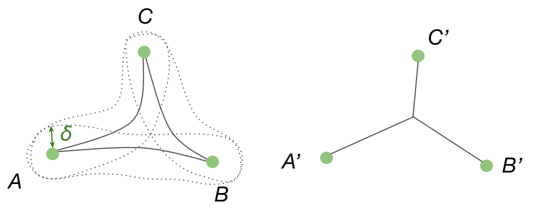

Figure 10: Example of a δ-slim triangle, where each side of $\triangle ABC$ is the geodesic distance of two points in the metric space.

Table 4: Linear classification accuracy using SupCon [39] as ℓ_{Flat}.

Dataset	Method (SupCon)	Fine Accuracy (↑)
CIFAR10	Flat	94.53
	ℓ_2-CPCC	95.08
	HypStructure (Ours)	**95.18**
CIFAR100	Flat	75.11
	ℓ_2-CPCC	75.66
	HypStructure (Ours)	**77.66**

C Additional Experimental Results

C.1 Results using Linear Evaluation

We also perform an evaluation of the *fine* classification accuracy following the common linear evaluation protocol [39] where a linear classifier is trained on top of the normalized penultimate layer features. We report these accuracies for the models trained on the CIFAR10 and CIFAR100 datasets in Table 4 for the leaf-only variants of the models. We observe that the relative trend of accuracies is identical to the ones reported using the kNN evaluation in Table 1 and our proposed method HypStructure outperforms the *flat* and ℓ_2-CPCC methods on both the datasets.

C.2 Component-wise Ablation Study of HypStructure

To understand the role of each component in our proposed methodology HypStructure, we perform a detailed ablation study with the different components and measure the *fine* and the *coarse* accuracies on the CIFAR100 dataset. Specifically, we examine

1. the role of embedding all internal nodes in the label hierarchy (eq. (8) and line 10 in Algorithm 1), as opposed to only using leaf nodes as in [104]. We refer to the inclusion of internal nodes as $\mathcal{T}_{\text{int}}$.
2. the role of hyperbolic class centroids computation using hyperbolic averaging (eq. (6) and line 8 in Algorithm 1), as opposed to the Euclidean computation of class prototypes as in [104]. We refer to the hyperbolic class centroid computation as ω_{hyp}.
3. the role of the hyperbolic centering loss in our proposed methodology (eq. (8) and line 11 in Algorithm 1), as opposed to not using a centering loss. We refer to the inclusion of the centering loss as ℓ_{center}.

We ablate over the aforementioned settings, where a ✓ denotes the inclusion of that setting, and report the results on the CIFAR100 dataset in Table 5. Firstly, we observe that while the centering loss ℓ_{center} improves the coarse accuracy only by a small increment, it leads to a significant improvement in the fine accuracy (rows $1 \rightarrow 2$ and $4 \rightarrow 5$), indicating that the centering of the root in the poincare disk allows for a better relative positioning of the fine classes within the coarse class groups. Secondly, we observe that both the inclusion of internal nodes $\mathcal{T}_{\text{int}}$, and the hyperbolic computation of the class centroids ω_{hyp} is critical for accurately embedding the hierarchy, and removing either of these components (i.e. rows $5 \rightarrow 3$ for $\mathcal{T}_{\text{int}}$ and rows $5 \rightarrow 2$ for ω_{hyp}), leads to a degradation in both the fine as well as the coarse accuracies. The best overall performance is observed when all three of the components are included (row 5).

Table 5: Ablation study on the components of `HypStructure`. We report the Classification accuracies based on the CIFAR100 model trained with ResNet-34.

`HypStructure` **Components**			**Classification Acc.↑**	
Internal Nodes ($\mathcal{T}_{\text{int}}$)	**Hyp. Class Centroids** (ω_{hyp})	**Hyp. Centering** (ℓ_{center})	**Fine**	**Coarse**
✓			75.03	84.77
✓		✓	75.61	84.81
	✓	✓	76.22	85.70
✓	✓		76.59	**86.23**
✓	✓	✓	**76.91**	86.22

C.3 OOD detection

C.3.1 Related Work and Methods

The goal of prior works in the OOD literature is the supervised setting of learning an accurate classifier for ID data, along with an ID-OOD detection methodology and this task has been explored in the generative model setting [42, 63, 71, 77, 97], and more extensively in the supervised discriminative model setting [2, 30, 36, 37, 51, 53, 82, 60]. The methods in this setting can be categorized into four sub-categories following [106], primarily:

Post-Hoc Inference These methods design post-processing/scoring mechanisms on base classifiers such as MSP [30], ODIN [51], ReAct [82], SSD+ [76], KNN+ [83] and RankFeat [80].

Training without outlier data These methods involve training-time regularization or different objective functions for improving OOD detection capabilities such as G-ODIN [36], CSI [85], LogitNorm [92] and CIDER [61].

Training with outlier data These methods assume access to auxiliary OOD training samples such as OE [31] and MixOE [105].

Data Augmentation These methods improve the generalization ability of image classifiers such as StyleAugment [22], AugMix [32] and RegMixup [69].

Our proposed work can be considered primarily in the **Training without outlier data** category, and we note that none of the prior works use any additional structural regularization term in the objective functions.

C.3.2 Dataset-wise OOD Detection Results

Table 6: Results on CIFAR10. OOD detection performance for ResNet-18 trained on CIFAR10. Training with `HypStructure` achieves strong OOD detection performance.

Method	**OOD Dataset AUROC (↑)**					**Avg. (↑)**
	SVHN	Textures	Places365	LSUN	iSUN	
ProxyAnchor	94.55	93.16	92.06	97.02	96.56	94.67
CE + SimCLR	99.22	96.56	86.70	85.60	86.78	90.97
CSI	94.69	94.87	93.04	97.93	98.01	95.71
CIDER	99.72	96.85	94.09	99.01	**96.64**	97.26
SSD+	99.51	98.35	**95.57**	97.83	95.67	97.38
KNN+	99.61	97.43	94.88	98.01	96.21	97.22
ℓ_2-CPCC	93.27	94.76	60.15	75.29	59.87	76.67
`HypStructure` (Ours)	**99.75**	**98.89**	94.80	**99.67**	95.64	**97.75**

We report the dataset-wise OOD detection results in Tables 7a, 6 and 7 for CIFAR100, CIFAR10 and ImageNet100 respectively. We compare with several other state-of-the-art baseline OOD detection

Table 7: Results on ImageNet100. OOD detection performance for ResNet-34 trained on ImageNet100. Training with `HypStructure` achieves strong OOD detection performance.

Method	**OOD Dataset AUROC (↑)**				**Avg. (↑)**
	SUN	Places365	Textures	iNaturalist	
CIDER	91.63	89.29	97.98	96.35	93.81
SSD+	88.97	85.98	**98.49**	96.42	92.46
KNN+	89.48	86.64	98.38	**96.46**	92.74
ℓ_2-CPCC	90.95	86.87	97.41	90.08	91.33
`HypStructure` (Ours)	**92.21**	**90.12**	97.33	95.61	**93.83**

methods for CIFAR10 and CIFAR100, namely ProxyAnchor [41], SimCLR [7] CSI [85], and CIDER [61] respectively. Results for these methods are taken from CIDER [61] where contrastive learning based OOD detection methods typically outperforms non-contrastive learning ones. For ImageNet100, in the absence of the available class ids used to train the original models in CIDER [61], we finetune the ResNet34 models on the created ImageNet100 dataset. For CIDER and SupCon, we use the official implementations and hyperparameters provided by the authors.

We observe that our proposed method leads to an improvement in the average OOD detection AUROC over all the ID datasets. In practice, we find that the Euclidean-centroid computational variant (first compute the Euclidean centroids and then apply the exponential map) of our proposed method performs slightly better than the hyperbolic-centroid computational variant (first apply the exponential map and then compute the hyperbolic average), for the specific task of OOD detection, while having equivalent performance on the ID classification task. Hence, we report the OOD detection accuracy corresponding to the first version.

C.4 Visualization of Learned Features

We provide additional visualizations of the learnt features from our proposed method `HypStructure` on the CIFAR10, CIFAR100 and ImageNet100 datasets in Figures 11, 12 and 13 respectively.

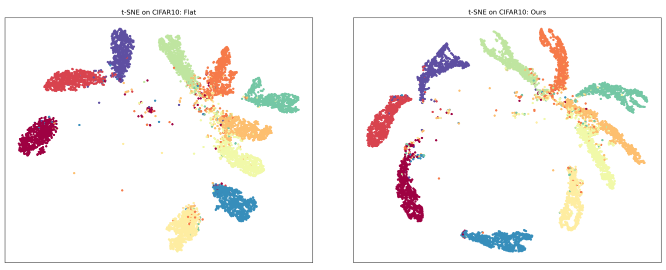

(a) (b)

Figure 11: Euclidean t-SNE Visualizations on CIFAR10.

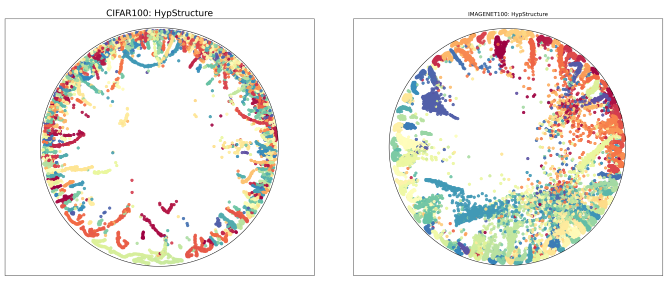

(a) (b)

Figure 12: Hyperbolic UMAP Visualizations on CIFAR100 and ImageNet100.

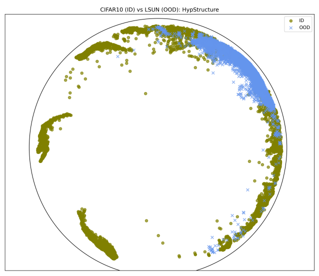

(a) (b)

Figure 13: Hyperbolic UMAP Visualizations of ID-OOD separation on CIFAR10 and ImageNet100.

C.5 Effect of Centering Loss and Embedding Internal Node

Embedding the internal tree nodes in `HypStructure` $\mathcal{T}_{\text{int}}$ (as compared to only leaf nodes in prior work CPCC) and placing the root node at the center of the Poincaré disk with ℓ_{center} loss, helps in embedding the hierarchy more accurately. To understand the impact of these components, we first visualize the learnt representations from `HypStructure`, with and without these components - i.e. embedding internal nodes and a centering loss vs leaf only nodes, via UMAP in Figure 14 (CIFAR100) and Figure 15 (ImageNet100). We also provide a performance comparison (fine accuracy) in Table 8.

Method	**CIFAR10**	**CIFAR100**	**ImageNet100**
`HypStructure` (leaf only)	94.54	76.22	89.85
`HypStructure` (with internal nodes and centering)	**94.79**	**76.68**	**90.12**

Table 8: Fine accuracy comparison of `HypStructure` with vs. without internal nodes and centering on CIFAR10, CIFAR100, and ImageNet100 datasets.

First, based on Figures Figure 14 and Figure 15, one can note that in the leaf-only setting without embedding internal nodes and centering loss (figures on the left), the samples belonging to the fine classes which share the same parent (same color) are in close proximity reflecting the hierarchy accurately, however the samples are not spread evenly. With the embedding of internal nodes and a centering loss (right), we note that the representations are spread between the center (root) to the boundary as well as across the Poincaré disk, which is more representative of the original hierarchy. This also leads to performance improvements as can be seen in Table 8.

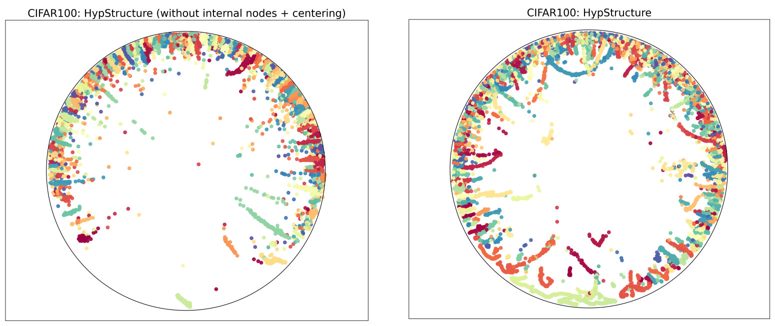

(a) (b)

Figure 14: Hyperbolic UMAP Visualizations on CIFAR100 using `HypStructure` without embedding the internal nodes and a hyperbolic centering loss (left), and with embedding the internal nodes along with a centering loss (right).

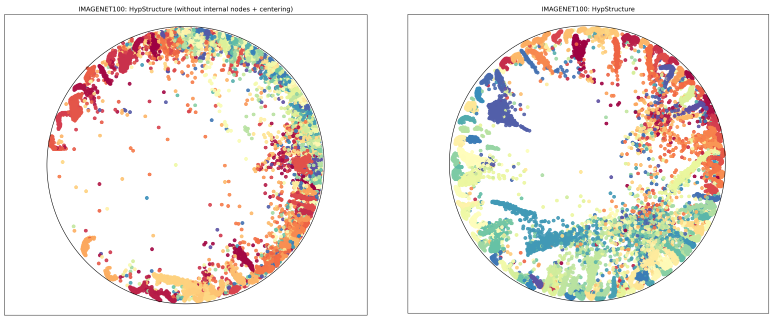

(a) (b)

Figure 15: Hyperbolic UMAP Visualizations on ImageNet100 using `HypStructure` without embedding the internal nodes and a hyperbolic centering loss (left), and with embedding the internal nodes along with a centering loss (right).

C.6 Effect of Label Hierarchy Weights

Compared to ranking-based hyperbolic losses [66], our HypCPCC factors in absolute values of the node-to-node distances. The learned hierarchy with HypCPCC will not only implicitly encode the correct parent-child relations, but can also learn more complex and weighted hierarchical relationships more accurately. To demonstrate this, we modify the CIFAR10 tree hierarchy, and gradually increase the weight for the left transportation branch to $2\times$ and $4\times$ and use new weighted trees for the CPCC tree distance computation. We visualize the learnt representations in Figure 16 and we can observe that in the learned representations from left to right, the distance between the transportation classes (blue) are larger as compared to other classes, as expected.

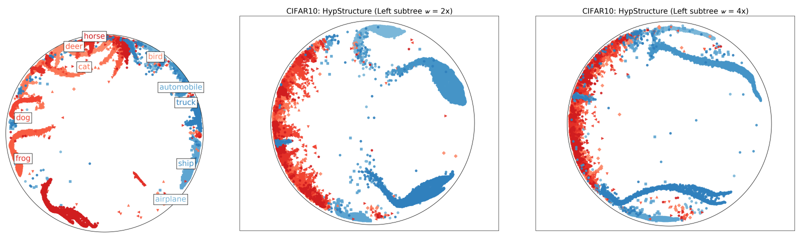

(a) (b) (c)

Figure 16: HypStructure can learn more nuanced representations with weighted hierarchy trees. Hyperbolic UMAP visualizations on CIFAR10 using HypStructure with differently weighted left-subtrees.

C.7 Effect of Klein Averaging

We experiment with the two HypCPCC variants, using Klein Averaging or Euclidean mean for centroid computation, as mentioned in Section 3.2 and report the results in Table 9. We empirically observe that using the Klein averaging leads to performance improvements across datasets.

Method	**CIFAR10**	**CIFAR100**	**ImageNet100**
Euclidean	94.56	75.64	90.08
Klein	**94.79**	**76.68**	**90.12**

Table 9: Fine accuracy comparison between Euclidean and Klein centroid computation methods in HypCPCC on CIFAR10, CIFAR100, and ImageNet100 datasets.

C.8 Experiments with the Hyperbolic Supervised Contrastive Loss

We experiment with the Hyperbolic Supervised Contrastive Loss as proposed in [21] as the choice of the ℓ_{Flat} loss and refer to this loss as $\ell_{\text{HypSupCon}}$. We follow the original setup as described by the authors for the measurement of the $\ell_{\text{HypSupCon}}$, where the representations from the encoders are not normalized directly, instead an exponential map is used to project these features from the Euclidean space to the Poincaré ball first. Then, the inner product measurement in the ℓ_{SupCon} is replaced with the negative hyperbolic distances in the Poincaré ball to compute the $\ell_{\text{HypSupCon}}$ loss. We also experiment with our proposed methodology `HypStructure` along with the $\ell_{\text{HypSupCon}}$ loss and report the classification accuracies and hierarchy embedding metrics for both these settings in Table 10. We further report the OOD detection performance on CIFAR10, CIFAR100 and ImageNet100 as in-distribution datasets for both of these settings in Tables 11, 12 and 13 respectively. We observe that using `HypStructure` with a hyperbolic loss such as $\ell_{\text{HypSupCon}}$ as the Flat loss leads to improvements in accuracy across classification and OOD detection tasks while also improving the quality of embedding the hierarchy. This demonstrates the wide applicability of our proposed method `HypStructure` which can be used in conjunction with both euclidean and non-euclidean classification losses.

Table 10: Evaluation of hierarchical information distortion and classification accuracy using `HypSupCon` [21] as ℓ_{Flat}. All metrics are reported as mean (standard deviation) over 3 seeds.

Dataset (Backbone)	**Method**	**Distortion of Hierarchy**		**Classification Accuracy**	
		δ_{rel} (↓)	**CPCC (↑)**	**Fine (↑)**	**Coarse (↑)**
CIFAR10 (ResNet-18)	Flat	0.128 (0.007)	0.745 (0.017)	94.58 (0.04)	98.96 (0.01)
	`HypStructure`	**0.017 (0.001)**	**0.989 (0.001)**	**95.04 (0.02)**	**99.36 (0.02)**
CIFAR100 (ResNet-34)	Flat	0.168 (0.002)	0.664 (0.012)	75.81 (0.06)	85.26 (0.07)
	`HypStructure`	**0.112 (0.005)**	**0.773 (0.008)**	**76.22 (0.14)**	**85.83 (0.06)**
ImageNet100 (ResNet-34)	Flat	0.157 (0.004)	0.473 (0.004)	89.87 (0.01)	90.41 (0.01)
	`HypStructure`	**0.126 (0.002)**	**0.714 (0.003)**	**90.26 (0.01)**	**90.95 (0.01)**

Table 11: Results on CIFAR10 when using the `HypSupCon`[21] as ℓ_{Flat} using ResNet-18 as the backbone. Training with `HypStructure` achieves improvements in OOD detection performance.

Method	**OOD Dataset AUROC (↑)**					**Avg. (↑)**
	SVHN	Textures	Places365	LSUN	iSUN	
$\ell_{\text{HypSupCon}}$	89.45	93.39	90.18	98.18	91.31	92.51
$\ell_{\text{HypSupCon}}$ + `HypStructure` (Ours)	**91.11**	**94.45**	**93.52**	**99.05**	**95.24**	**94.68**

Table 12: Results on CIFAR100 when using the `HypSupCon`[21] as ℓ_{Flat} using ResNet-34 as the backbone. Training with `HypStructure` achieves improvements in OOD detection performance.

Method	**OOD Dataset AUROC (↑)**					**Avg. (↑)**
	SVHN	Textures	Places365	LSUN	iSUN	
$\ell_{\text{HypSupCon}}$	80.16	79.61	74.02	70.22	82.35	77.27
$\ell_{\text{HypSupCon}}$ + `HypStructure` (Ours)	**82.28**	**83.51**	**77.95**	**86.64**	69.86	**80.05**

C.9 Experiments with a Hyperbolic Backbone

We experiment with Clipped Hyperbolic Neural Networks (HNNs) [26] as a hyperbolic backbone and use our proposed methodology `HypStructure` in conjunction with the hyperbolic Multinomial Logistic Regression (MLR) loss. We report the classification accuracies and hierarchy embedding metrics on the CIFAR10 and CIFAR100 datasets in Table 14, and the OOD detection performances using CIFAR10 and CIFAR100 as in-distribution datasets in Tables 15 and 16 respectively. We observe that using `HypStructure` along with a hyperbolic backbone leads to improvements in classification accuracies, reduced distortion in embedding the hierarchy, and improved OOD detection performance overall, demonstrating the wide applicability of `HypStructure` with hyperbolic networks.

Table 13: Results on ImageNet100 when using the `HypSupCon`[21] as ℓ_{Flat} using ResNet-34 as the backbone. Training with `HypStructure` achieves improvements in OOD detection performance.

Method	**OOD Dataset AUROC (↑)**				**Avg. (↑)**
	SUN	Places365	Textures	iNaturalist	
$\ell_{\text{HypSupCon}}$	91.96	90.74	**97.42**	94.04	93.54
$\ell_{\text{HypSupCon}}$ + `HypStructure` (Ours)	**93.87**	**91.56**	97.04	**95.16**	**94.41**

Table 14: Evaluation of hierarchical information distortion and classification accuracy using Clipped Hyperbolic Neural Networks [26] as the backbone. All metrics are reported as mean (standard deviation) over 3 seeds.

Dataset (Backbone)	**Method**	**Distortion of Hierarchy**		**Classification Accuracy**	
		δ_{rel} (↓)	**CPCC** (↑)	**Fine** (↑)	**Coarse** (↑)
CIFAR10 (Clipped HNN [26])	Flat	0.084 (0.008)	0.604 (0.004)	94.81 (0.23)	89.71 (2.04)
	`HypStructure`	**0.013 (0.002)**	**0.988 (0.001)**	**94.97 (0.12)**	**98.35 (0.22)**
CIFAR100 (Clipped HNN [26])	Flat	0.098 (0.001)	0.528 (0.009)	76.46 (0.26)	49.26 (0.73)
	`HypStructure`	**0.064 (0.006)**	**0.624 (0.005)**	**77.96 (0.14)**	**55.46 (0.61)**

Table 15: Results on CIFAR10 when using the Clipped Hyperbolic Neural Networks [26] as the backbone. Training with `HypStructure` achieves improvements in OOD detection performance.

Method	**OOD Dataset AUROC (↑)**					**Avg. (↑)**
	SVHN	Textures	Places365	LSUN	iSUN	
Clipped HNN [26]	92.63	90.74	88.46	95.66	92.41	91.98
Clipped HNN [26] + `HypStructure` (Ours)	**95.41**	**93.91**	**92.31**	**96.87**	**94.92**	**94.68**

Table 16: Results on CIFAR100 when using the Clipped Hyperbolic Neural Networks [26] as the backbone. Training with `HypStructure` achieves improvements in OOD detection performance.

Method	**OOD Dataset AUROC (↑)**					**Avg. (↑)**
	SVHN	Textures	Places365	LSUN	iSUN	
Clipped HNN [26]	89.94	83.77	77.26	82.87	82.35	83.23
Clipped HNN [26] + `HypStructure` (Ours)	**91.56**	**84.31**	**78.45**	**87.53**	**83.44**	**85.06**

NeurIPS Paper Checklist

1. **Claims**

   Question: Do the main claims made in the abstract and introduction accurately reflect the paper's contributions and scope?

   Answer: [Yes]

   Justification: The abstract and the introduction both clearly state the claims made by the paper, along with a clear description of the contributions, assumptions and limitations.

   Guidelines:

   - The answer NA means that the abstract and introduction do not include the claims made in the paper.
   - The abstract and/or introduction should clearly state the claims made, including the contributions made in the paper and important assumptions and limitations. A No or NA answer to this question will not be perceived well by the reviewers.
   - The claims made should match theoretical and experimental results, and reflect how much the results can be expected to generalize to other settings.
   - It is fine to include aspirational goals as motivation as long as it is clear that these goals are not attained by the paper.

2. **Limitations**

   Question: Does the paper discuss the limitations of the work performed by the authors?

   Answer: [Yes]

   Justification: Yes, the limitations of the current work as well as the avenues for future improvements to the current work can be found in Section 7.

   Guidelines:

   - The answer NA means that the paper has no limitation while the answer No means that the paper has limitations, but those are not discussed in the paper.
   - The authors are encouraged to create a separate "Limitations" section in their paper.
   - The paper should point out any strong assumptions and how robust the results are to violations of these assumptions (e.g., independence assumptions, noiseless settings, model well-specification, asymptotic approximations only holding locally). The authors should reflect on how these assumptions might be violated in practice and what the implications would be.
   - The authors should reflect on the scope of the claims made, e.g., if the approach was only tested on a few datasets or with a few runs. In general, empirical results often depend on implicit assumptions, which should be articulated.
   - The authors should reflect on the factors that influence the performance of the approach. For example, a facial recognition algorithm may perform poorly when image resolution is low or images are taken in low lighting. Or a speech-to-text system might not be used reliably to provide closed captions for online lectures because it fails to handle technical jargon.
   - The authors should discuss the computational efficiency of the proposed algorithms and how they scale with dataset size.
   - If applicable, the authors should discuss possible limitations of their approach to address problems of privacy and fairness.
   - While the authors might fear that complete honesty about limitations might be used by reviewers as grounds for rejection, a worse outcome might be that reviewers discover limitations that aren't acknowledged in the paper. The authors should use their best judgment and recognize that individual actions in favor of transparency play an important role in developing norms that preserve the integrity of the community. Reviewers will be specifically instructed to not penalize honesty concerning limitations.

3. **Theory Assumptions and Proofs**

   Question: For each theoretical result, does the paper provide the full set of assumptions and a complete (and correct) proof?

Answer: [Yes]

Justification: Yes, for all the main results of the paper in Section 5, a full set of assumptions and a complete proof is provided in Section A in the Appendix.

Guidelines:

- The answer NA means that the paper does not include theoretical results.
- All the theorems, formulas, and proofs in the paper should be numbered and cross-referenced.
- All assumptions should be clearly stated or referenced in the statement of any theorems.
- The proofs can either appear in the main paper or the supplemental material, but if they appear in the supplemental material, the authors are encouraged to provide a short proof sketch to provide intuition.
- Inversely, any informal proof provided in the core of the paper should be complemented by formal proofs provided in appendix or supplemental material.
- Theorems and Lemmas that the proof relies upon should be properly referenced.

4. **Experimental Result Reproducibility**

Question: Does the paper fully disclose all the information needed to reproduce the main experimental results of the paper to the extent that it affects the main claims and/or conclusions of the paper (regardless of whether the code and data are provided or not)?

Answer: [Yes]

Justification: Yes, the paper discloses all the necessary details about the implemented architectures used, hyperparameters for each setting, algorithm pseudocode and other experimental details to reproduce all the experiments in the paper. These details can be found in Section B in the Appendix.

Guidelines:

- The answer NA means that the paper does not include experiments.
- If the paper includes experiments, a No answer to this question will not be perceived well by the reviewers: Making the paper reproducible is important, regardless of whether the code and data are provided or not.
- If the contribution is a dataset and/or model, the authors should describe the steps taken to make their results reproducible or verifiable.
- Depending on the contribution, reproducibility can be accomplished in various ways. For example, if the contribution is a novel architecture, describing the architecture fully might suffice, or if the contribution is a specific model and empirical evaluation, it may be necessary to either make it possible for others to replicate the model with the same dataset, or provide access to the model. In general. releasing code and data is often one good way to accomplish this, but reproducibility can also be provided via detailed instructions for how to replicate the results, access to a hosted model (e.g., in the case of a large language model), releasing of a model checkpoint, or other means that are appropriate to the research performed.
- While NeurIPS does not require releasing code, the conference does require all submissions to provide some reasonable avenue for reproducibility, which may depend on the nature of the contribution. For example
  (a) If the contribution is primarily a new algorithm, the paper should make it clear how to reproduce that algorithm.
  (b) If the contribution is primarily a new model architecture, the paper should describe the architecture clearly and fully.
  (c) If the contribution is a new model (e.g., a large language model), then there should either be a way to access this model for reproducing the results or a way to reproduce the model (e.g., with an open-source dataset or instructions for how to construct the dataset).
  (d) We recognize that reproducibility may be tricky in some cases, in which case authors are welcome to describe the particular way they provide for reproducibility. In the case of closed-source models, it may be that access to the model is limited in some way (e.g., to registered users), but it should be possible for other researchers to have some path to reproducing or verifying the results.

5. **Open access to data and code**

   Question: Does the paper provide open access to the data and code, with sufficient instructions to faithfully reproduce the main experimental results, as described in supplemental material?

   Answer: [Yes]

   Justification: The paper includes the specific instructions to access the datasets used for all the experimentation. These can be found in Section B in the Appendix. The code for this project is released to the public.

   Guidelines:

   - The answer NA means that paper does not include experiments requiring code.
   - Please see the NeurIPS code and data submission guidelines (`https://nips.cc/public/guides/CodeSubmissionPolicy`) for more details.
   - While we encourage the release of code and data, we understand that this might not be possible, so "No" is an acceptable answer. Papers cannot be rejected simply for not including code, unless this is central to the contribution (e.g., for a new open-source benchmark).
   - The instructions should contain the exact command and environment needed to run to reproduce the results. See the NeurIPS code and data submission guidelines (`https://nips.cc/public/guides/CodeSubmissionPolicy`) for more details.
   - The authors should provide instructions on data access and preparation, including how to access the raw data, preprocessed data, intermediate data, and generated data, etc.
   - The authors should provide scripts to reproduce all experimental results for the new proposed method and baselines. If only a subset of experiments are reproducible, they should state which ones are omitted from the script and why.
   - At submission time, to preserve anonymity, the authors should release anonymized versions (if applicable).
   - Providing as much information as possible in supplemental material (appended to the paper) is recommended, but including URLs to data and code is permitted.

6. **Experimental Setting/Details**

   Question: Does the paper specify all the training and test details (e.g., data splits, hyperparameters, how they were chosen, type of optimizer, etc.) necessary to understand the results?

   Answer: [Yes]

   Justification: Yes, the paper uses standard data splits from publicly available benchmark sources and provides details regarding the choice of hyperparameters, optimizer and other decisions necessary for understanding the results. These details can be found in Section B in the Appendix.

   Guidelines:

   - The answer NA means that the paper does not include experiments.
   - The experimental setting should be presented in the core of the paper to a level of detail that is necessary to appreciate the results and make sense of them.
   - The full details can be provided either with the code, in appendix, or as supplemental material.

7. **Experiment Statistical Significance**

   Question: Does the paper report error bars suitably and correctly defined or other appropriate information about the statistical significance of the experiments?

   Answer: [Yes]

   Justification: Yes, the paper reports the error bars and other information about the statistical significance of the results in the Section 4 in the main paper.

   Guidelines:

   - The answer NA means that the paper does not include experiments.

- The authors should answer "Yes" if the results are accompanied by error bars, confidence intervals, or statistical significance tests, at least for the experiments that support the main claims of the paper.
- The factors of variability that the error bars are capturing should be clearly stated (for example, train/test split, initialization, random drawing of some parameter, or overall run with given experimental conditions).
- The method for calculating the error bars should be explained (closed form formula, call to a library function, bootstrap, etc.)
- The assumptions made should be given (e.g., Normally distributed errors).
- It should be clear whether the error bar is the standard deviation or the standard error of the mean.
- It is OK to report 1-sigma error bars, but one should state it. The authors should preferably report a 2-sigma error bar than state that they have a 96% CI, if the hypothesis of Normality of errors is not verified.
- For asymmetric distributions, the authors should be careful not to show in tables or figures symmetric error bars that would yield results that are out of range (e.g. negative error rates).
- If error bars are reported in tables or plots, The authors should explain in the text how they were calculated and reference the corresponding figures or tables in the text.

8. **Experiments Compute Resources**

   Question: For each experiment, does the paper provide sufficient information on the computer resources (type of compute workers, memory, time of execution) needed to reproduce the experiments?

   Answer: [Yes]

   Justification: Yes, the paper provides details about the compute resources, hardware and software needed to reproduce the experiments in Section B of the Appendix.

   Guidelines:

   - The answer NA means that the paper does not include experiments.
   - The paper should indicate the type of compute workers CPU or GPU, internal cluster, or cloud provider, including relevant memory and storage.
   - The paper should provide the amount of compute required for each of the individual experimental runs as well as estimate the total compute.
   - The paper should disclose whether the full research project required more compute than the experiments reported in the paper (e.g., preliminary or failed experiments that didn't make it into the paper).

9. **Code Of Ethics**

   Question: Does the research conducted in the paper conform, in every respect, with the NeurIPS Code of Ethics `https://neurips.cc/public/EthicsGuidelines`?

   Answer: [Yes]

   Justification: Yes, the research conducted in this paper conforms in every respect, with the NeurIPS code of ethics.

   Guidelines:

   - The answer NA means that the authors have not reviewed the NeurIPS Code of Ethics.
   - If the authors answer No, they should explain the special circumstances that require a deviation from the Code of Ethics.
   - The authors should make sure to preserve anonymity (e.g., if there is a special consideration due to laws or regulations in their jurisdiction).

10. **Broader Impacts**

    Question: Does the paper discuss both potential positive societal impacts and negative societal impacts of the work performed?

    Answer: [Yes]

Justification: We discuss the potential positive and negative societal impacts of our work in Section B.1 of the Appendix.

Guidelines:

- The answer NA means that there is no societal impact of the work performed.
- If the authors answer NA or No, they should explain why their work has no societal impact or why the paper does not address societal impact.
- Examples of negative societal impacts include potential malicious or unintended uses (e.g., disinformation, generating fake profiles, surveillance), fairness considerations (e.g., deployment of technologies that could make decisions that unfairly impact specific groups), privacy considerations, and security considerations.
- The conference expects that many papers will be foundational research and not tied to particular applications, let alone deployments. However, if there is a direct path to any negative applications, the authors should point it out. For example, it is legitimate to point out that an improvement in the quality of generative models could be used to generate deepfakes for disinformation. On the other hand, it is not needed to point out that a generic algorithm for optimizing neural networks could enable people to train models that generate Deepfakes faster.
- The authors should consider possible harms that could arise when the technology is being used as intended and functioning correctly, harms that could arise when the technology is being used as intended but gives incorrect results, and harms following from (intentional or unintentional) misuse of the technology.
- If there are negative societal impacts, the authors could also discuss possible mitigation strategies (e.g., gated release of models, providing defenses in addition to attacks, mechanisms for monitoring misuse, mechanisms to monitor how a system learns from feedback over time, improving the efficiency and accessibility of ML).

11. **Safeguards**

    Question: Does the paper describe safeguards that have been put in place for responsible release of data or models that have a high risk for misuse (e.g., pretrained language models, image generators, or scraped datasets)?

    Answer: [NA]

    Justification: The paper uses publicly available datasets, and does not release any data or code that have a risk of misuse.

    Guidelines:

    - The answer NA means that the paper poses no such risks.
    - Released models that have a high risk for misuse or dual-use should be released with necessary safeguards to allow for controlled use of the model, for example by requiring that users adhere to usage guidelines or restrictions to access the model or implementing safety filters.
    - Datasets that have been scraped from the Internet could pose safety risks. The authors should describe how they avoided releasing unsafe images.
    - We recognize that providing effective safeguards is challenging, and many papers do not require this, but we encourage authors to take this into account and make a best faith effort.

12. **Licenses for existing assets**

    Question: Are the creators or original owners of assets (e.g., code, data, models), used in the paper, properly credited and are the license and terms of use explicitly mentioned and properly respected?

    Answer: [Yes]

    Justification: We have appropriately cited the original owners of data and code which is used in the paper.

    Guidelines:

    - The answer NA means that the paper does not use existing assets.
    - The authors should cite the original paper that produced the code package or dataset.

- The authors should state which version of the asset is used and, if possible, include a URL.
- The name of the license (e.g., CC-BY 4.0) should be included for each asset.
- For scraped data from a particular source (e.g., website), the copyright and terms of service of that source should be provided.
- If assets are released, the license, copyright information, and terms of use in the package should be provided. For popular datasets, `paperswithcode.com/datasets` has curated licenses for some datasets. Their licensing guide can help determine the license of a dataset.
- For existing datasets that are re-packaged, both the original license and the license of the derived asset (if it has changed) should be provided.
- If this information is not available online, the authors are encouraged to reach out to the asset's creators.

13. **New Assets**

    Question: Are new assets introduced in the paper well documented and is the documentation provided alongside the assets?

    Answer: [NA]

    Justification: The paper does not release any new assets.

    Guidelines:

    - The answer NA means that the paper does not release new assets.
    - Researchers should communicate the details of the dataset/code/model as part of their submissions via structured templates. This includes details about training, license, limitations, etc.
    - The paper should discuss whether and how consent was obtained from people whose asset is used.
    - At submission time, remember to anonymize your assets (if applicable). You can either create an anonymized URL or include an anonymized zip file.

14. **Crowdsourcing and Research with Human Subjects**

    Question: For crowdsourcing experiments and research with human subjects, does the paper include the full text of instructions given to participants and screenshots, if applicable, as well as details about compensation (if any)?

    Answer: [NA]

    Justification: The paper does not involve crowdsourcing, nor research with human subjects.

    Guidelines:

    - The answer NA means that the paper does not involve crowdsourcing nor research with human subjects.
    - Including this information in the supplemental material is fine, but if the main contribution of the paper involves human subjects, then as much detail as possible should be included in the main paper.
    - According to the NeurIPS Code of Ethics, workers involved in data collection, curation, or other labor should be paid at least the minimum wage in the country of the data collector.

15. **Institutional Review Board (IRB) Approvals or Equivalent for Research with Human Subjects**

    Question: Does the paper describe potential risks incurred by study participants, whether such risks were disclosed to the subjects, and whether Institutional Review Board (IRB) approvals (or an equivalent approval/review based on the requirements of your country or institution) were obtained?

    Answer: [NA]

    Justification: The paper does not involve crowdsourcing nor research with human subjects.

    Guidelines:

- The answer NA means that the paper does not involve crowdsourcing nor research with human subjects.
- Depending on the country in which research is conducted, IRB approval (or equivalent) may be required for any human subjects research. If you obtained IRB approval, you should clearly state this in the paper.
- We recognize that the procedures for this may vary significantly between institutions and locations, and we expect authors to adhere to the NeurIPS Code of Ethics and the guidelines for their institution.
- For initial submissions, do not include any information that would break anonymity (if applicable), such as the institution conducting the review.